TABLE II

RESULTING HEMODYNAMIC PARAMETERS.

Variable	Target	Simulation results
HR(bpm)	115-150	150
LVEDV(ml)	42-65	53
LVEDP(mmHg)	3.6-16.1	4-10
LVESV(ml)	21-40	43.7-48.4
LVESP(mmHg)	69-110	43.9-65.1

HR:Heart rate, LVEDV:left ventricular end-diastolic volume, LVEDP:left ventricular end-diastolic pressure, LVESV:left ventricular end-systolic volume, LVESP:left ventricular end-systolic pressure

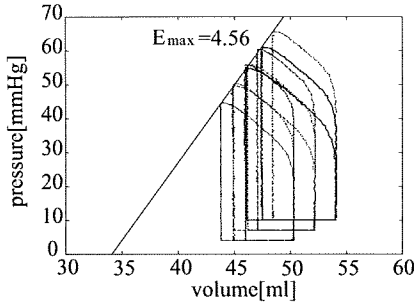

Fig. 8. Resulting pressure volume loop under 9 preload and afterload.

TABLE III

ATP CONSUMPTION AND AREA OF PRESSURE VOLUME LOOP.

pre-load	after-load	ATP_{CB}	ATP_{other}	ATP_{total}	EW	PE	PVA
4.0	2000	22.9	37.0	59.9	206	186	407
4.0	3000	24.3	37.0	61.3	219	213	449
4.0	4000	25.5	37.0	62.5	250	255	497
7.0	2000	24.7	37.0	61.7	221	231	476
7.0	3000	26.5	37.0	63.5	263	292	537
7.0	4000	27.7	37.0	64.7	273	313	572
10.0	2000	26.5	37.0	63.5	262	275	535
10.0	3000	28.4	37.0	65.4	281	323	595
10.0	4000	29.8	37.0	66.8	282	370	643

Units: preload, [mmHg]; afterload, [mmHg·msec/ml]; ATP, [mM]; EW, PE, PVA, [ml·mmHg].

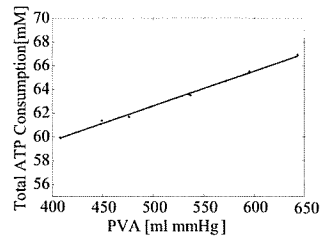

Fig. 9. Resulting relation between PVA and total ATP consumption.

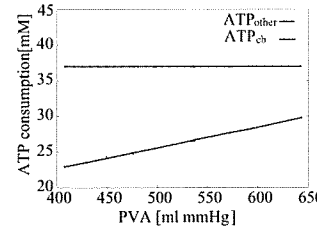

Fig. 10. Resulting relation between PVA and ATP consumptions in cross-bridge and other components.

was 0.1[msec], and the total calculation time with IBM p690 (96CPU, PowerPC 1.5GHz) was about 60 min.

Resulting hemodynamic parameters are presented in Table II with the published experimental values [6][2][10]. Corresponding pressure volume loops are presented in Figure 8. From this result, we can recognize that all the end-systolic pressure volume point coincide in single line where R^2 was 0.989. Corresponding E_{max} was 4.56[mmHg/ml] for these results.

In Kyoto Model, ATP consumption is calculated at the crossbridge and the ion transporters. Here we define ATP_{CB} as the ATP consumption at the crossbridge, and ATP_{other} as the ATP consumption at the ion transporters. Resulting ATP consumption and EW, PE and PVA for different afterloads and preloads are presented in Table III. The relation between PVA and the total ATP consumption is presented in Fig.9. Also the relation between PVA and ATP_{CB}, ATP_{other} are presented in Fig.10. From these results we can recognize that only the crossbridge ATP consumption is linearly related to PVA. Note that there is no clear relation between the total ATP consumption and EW or PE.

VI. CONCLUSIONS

We proposed an approximation model of the crossbridge model which can be stably calculated by the weak coupling calculation. From the experimental results, the model showed very good agreement with the animal experimental results.

The results show that the model can be used for evaluating the energetics of heart. The results imply that the mechanism of the linear relation between PVA and ATP consumption is not simple since the relation between the PVA and EW or PE are not linear. The analysis of this relation is the important future work.

REFERENCES

[1] Suga, Takagi, Gotoh, Sunagawa: Heart Mechanics and its Energetics, Corona, pp.11, 2000. (in Japanese)

[2] Hiroyuki Suga, Ryuichi Hisano, Shunji Hirata, Takakazu Hayashi, Osamu Yamada, Ishio Ninomiya: Heart rate-independent energetics and systolic pressure-volume area in dog heart, *Am J Physiol Heart Circ Physiol*! $vol.244, pp.H211! $1983!%

[3] Kenji Sunagawa, W. Lowell Maughan, Daniel Burkhoff, Liichi Sagawa: Left ventricular interaction with arterial load studied in isolated canine ventricle, *Am J Physiol Heart Circ Physiol*! $vol.245, pp.H773! $1983!%

[4] S. L. Lindstedt, P. J. Schaeffer: Use of allometry in predicting anatomical and physiological parameters of mammals, *Laboratory Animals*, vol.36,pp.1-19,2002!%

[5] Satoshi Matsuoka, Nobuaki Sarai, Hikari Jo, Akinori Noma: Simulation of ATP metabolism in cardiac excitation-contraction coupling *Progress in Biophysics & Molecular Biology*, vol.85, pp.279-299, 2004.

[6] S. Solomon, S. Nikolic, S. Glantz, E. Yellin: Left ventricular diastolic function of remodeled myocardium in dogs with pacing-induced heart failure, *Am J Physiol Heart Circ Physiol*, vol.274, pp.H945-H954, 1998.

[7] Tokuda, Sekioka, Ueno, Hayashi, Havliecek: Numerical Simulator for Evaluation of Mechanical Function of Left Ventricle, Japan Society of Mechanical Engineering, Vol. 37, No. 1, pp.98-104, 1992. (in Japanese)

[8] N. Stergiopulos, B E. Westerrhof, N. Westerrhof: Total arterial inertance as the fourth element of the windkessel model, *Am J Physiol Heart Circ Physiol*, vol.276, pp.H81, 1999.

[9] Jorge A. Negroni, Elena C. Lascano: A Cardiac Muscle Model Relating Sarcomere Dynamics to Calcium Kinetics! $ *J Mol Cell Cardiol*, vol.28, pp.915-929, 1996.

[10] L. Carr McClain, Leon D. Wright, Raj K. Bose, John A. Spratt, George W. Maier: Afterload Sensitivity of Nonlinear End-Systolic Pressure-Volume Relation vs Preload Recruitable Stroke Work in Conscious Dogs, *J Surgical Research*, vol.75, pp.6-17, 1998.

nature chemistry

ARTICLES

PUBLISHED ONLINE: 23 SEPTEMBER 2009 | DOI: 10.1038/NCHEM.365

Self-assembling nanoprobes that display off/on ^{19}F nuclear magnetic resonance signals for protein detection and imaging

Yousuke Takaoka[1], Takashi Sakamoto[1], Shinya Tsukiji[1,4], Michiko Narazaki[2], Tetsuya Matsuda[2], Hidehito Tochio[3], Masahiro Shirakawa[3] and Itaru Hamachi[1,4]*

Magnetic resonance imaging (MRI) is one of the most promising techniques for the non-invasive visualization of biomarkers and biologically relevant species, both *in vivo* and *ex vivo*. Although ^{1}H MRI with paramagnetic contrast agents, such as Gd^{3+} complexes and iron oxide, is widely used, it often suffers from low contrast because of the large background signals caused by the abundant distribution of protons in biological samples. Here we report the use of supramolecular organic nanoparticles to detect specific proteins by ^{19}F-based MRI in an off/on mode. In NMR spectroscopy these designed probes are silent when aggregated, but in the presence of a target protein they disassemble to produce a sharp signal. This 'turn-on' response allowed us to visualize clearly the protein within live cells by ^{19}F MRI and construct an in-cell inhibitor assay. This recognition-driven disassembly of nanoprobes for a turn-on ^{19}F signal is unprecedented and may extend the use of ^{19}F MRI for specific protein imaging.

MRI is superior to optical bioimaging in living systems for the visualization of deep tissues[1–3]. Currently, ^{1}H MRI is widely used for diagnostic purposes because it is highly sensitive, which is attributed to the abundance of water molecules in the vicinity of contrast agents. However, ^{1}H MRI also often suffers from low contrast-to-noise ratio because of the large background signals from water protons. Therefore, for the specific imaging of biomarkers and biologically relevant molecules with higher functional and/or spatial resolution, both *in vivo* and *ex vivo*, there is still an obvious need to develop new methodologies.

Several approaches have been proposed[2–6]. In particular, ^{19}F holds great promise as an alternative nuclide for MRI as it is highly sensitive in nuclear magnetic resonance (NMR) spectroscopy (83% relative to ^{1}H) and has 100% natural abundance. A more important advantage of ^{19}F is that in animal bodies essentially no ^{19}F is detectable by NMR spectroscopy, which therefore eliminates interference from background signals[7,8]. As such, when a probe containing ^{19}F is applied to a biological sample, only the signal from the molecule can be detected. However, ^{19}F MRI technology is still in its infancy. Despite the significant importance for medical diagnosis, strategies to image specific proteins and/or enzymes with high MRI contrast are very limited.

To date, both targeting and switching probes have been proposed for ^{19}F NMR–MRI detection. The former is based on the accumulation of probes in specific regions in tissues through binding to localized components[9], and the latter provides signals that can be modulated by enzymatic reaction. Two types of switching ^{19}F MRI probes reported involve enzyme substrates: one displays chemical shift changes[10] and the other shows a signal turn-on dependent on paramagnetic relaxation enhancement on enzymatic cleavages[11]. The switching of these probes relies entirely on the catalytic activity of the enzymes, and thus the probes are spatially diffused away from the target enzyme and also not applicable for non-enzymatic protein targets. Therefore, more universal MRI strategies for protein detection and imaging that do not rely on enzymatic activities are highly desirable.

Here we describe a novel strategy to detect specific proteins with an 'off/on' type of signal in ^{19}F NMR spectroscopy using dynamic self-assembled nanoparticles. The basis of our idea is that the ^{19}F NMR signal is broadened and attenuated when the molecules assemble into aggregates of high molecular mass (M_r), but recovers on their disassembly. ^{19}F has a relatively large chemical shift anisotropy (approximately 39 ppm for a $-CF_3$ group)[12], so the transverse relaxation of signals in ^{19}F NMR spectroscopy is extremely sensitive to the apparent M_r because of the relaxation mechanism of chemical shift anisotropy. Thus, the formation of a large molecular assembly can cause severe broadening of the signal in ^{19}F NMR spectroscopy. Accordingly, small-molecule probes were designed that are composed of a ^{19}F-containing group and a ligand specific to the protein of interest, and concurrently equipped with the ability to form nanoaggregates. The probe alone is NMR-silent because of its self-assembly, but gives a distinct ^{19}F signal in response to the target protein through the binding-mediated disassembly of the probe (Fig. 1a). As the signal response is determined by specific protein–ligand interactions, this principle should be applicable to the detection of certain proteins, including both enzymes and non-enzymatic proteins.

For the proof-of-principle experiment, we initially chose human carbonic anhydrase I (hCAI) as a target protein. Probe **1** was synthesized to give a 3,5-bis(trifluoromethyl)benzene derivative that carries six magnetically equivalent ^{19}F nuclei connected to a benzenesulfonamide moiety, a ligand specific for hCAI (dissociation

[1]Department of Synthetic Chemistry and Biological Chemistry, Graduate School of Engineering, Kyoto University, Katsura, Nishikyo-ku, Kyoto 615-8510, Japan, [2]Department of Systems Science, Graduate School of Informatics, Kyoto University, 36-1 Yoshida-Honmachi, Sakyo-ku, Kyoto 606-8501, Japan, [3]Department of Molecular Engineering, Graduate School of Engineering, Kyoto University, Katsura, Nishikyo-ku, Kyoto 615-8510, Japan, [4]Core Research for Evolutional Science and Technology, Japan Science and Technology Agency, Sanbancho, Chiyodaku, Tokyo, 102-0075, Japan.
*e-mail: ihamachi@sbchem.kyoto-u.ac.jp

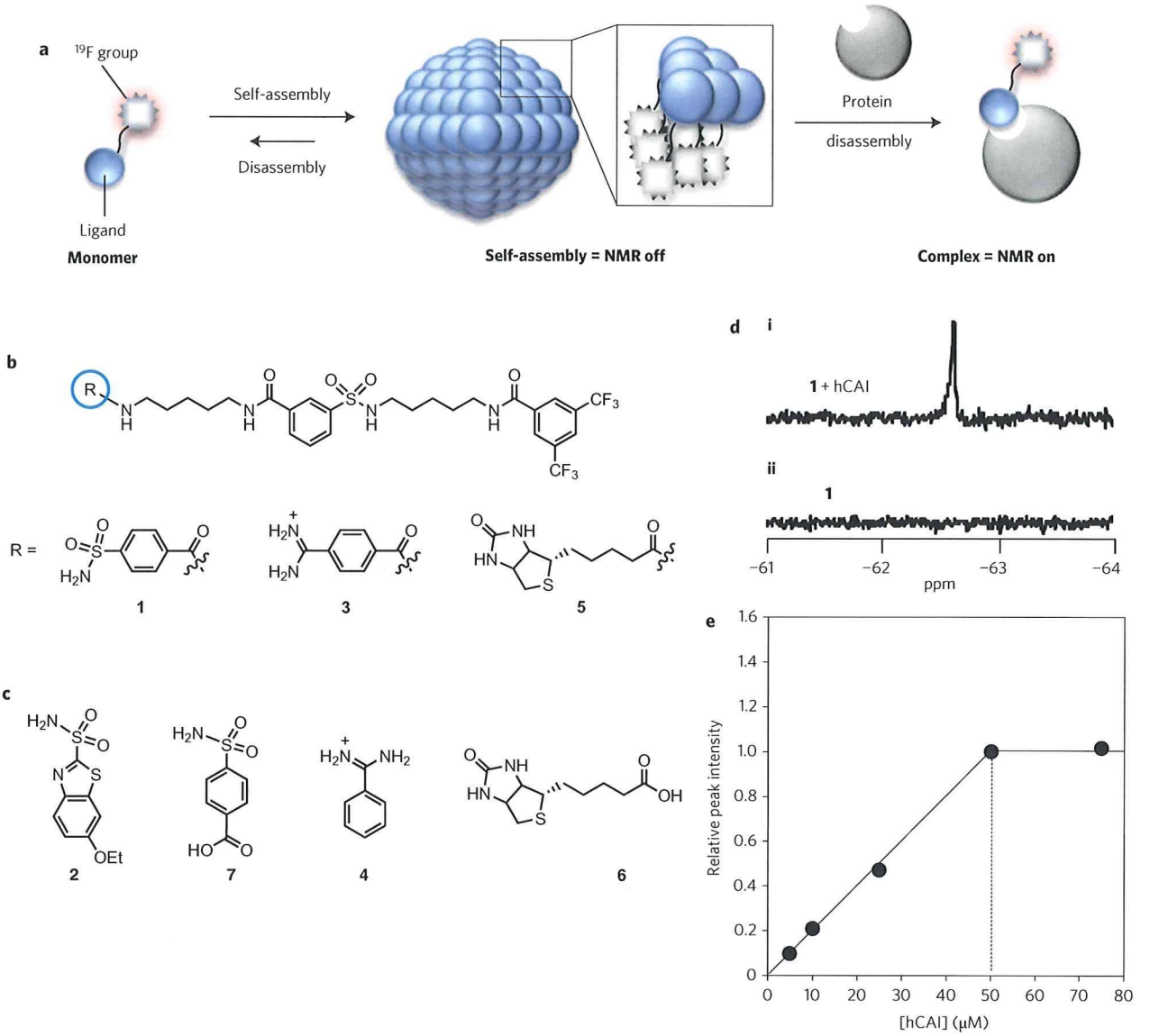

Figure 1 | Off/on ^{19}F NMR probes for protein imaging. a, Strategy used for an off/on switching mode of ^{19}F NMR. **b,** Chemical structures of probes **1**, **3** and **5** for hCAI, TPS and avidin, respectively. **c,** Chemical structures of enzyme inhibitors **2** and **7** for hCAI, **4** for TPS and ligand **6** for avidin. **d,** Turn-on ^{19}F NMR signal of probe **1** (50 μM) in the presence (**i**) or absence (**ii**) of hCAI (50 μM). The signal-to-noise ratio (SNR) was 60.1. **e,** Dependence of the ^{19}F-signal intensity (−62.6 ppm) on the hCAI concentration for probe **1** (50 μM) in 50 mM HEPES buffer (pH 7.2, 0.2 mM TFA as an internal standard for peak intensity and chemical shift, 10% D_2O (v/v)) at 25 °C.

constant K_d = ca. 3 μM) (ref. 13), by a relatively hydrophobic linker (Fig. 1b and Supplementary Information). When **1** was dissolved in a buffer solution that contained trifluoroacetic acid (TFA; internal standard at −75.6 ppm), no ^{19}F signal was observed. However, a sharp signal appeared at −62.6 ppm on the addition of hCAI (Fig. 1d). The signal intensity increased linearly in proportion to the concentration of hCAI, and was saturated at a 1:1 molar ratio of probe **1** and hCAI (Fig. 1e). On the subsequent addition of a strong inhibitor, ethoxzolamide (**2**, Fig. 1c)[14], into the above solution, the signal disappeared again (Supplementary Fig. 1a). These data indicate that (1) probe **1** alone is silent in NMR spectroscopy, (2) the ^{19}F signal can be assigned to probe **1** bound to the ligand-binding pocket of hCAI and (3) the signal can be turned off in a reversible manner when the probe is expelled from the protein (that is, when the target protein is incapable of binding the probe).

We next examined the target specificity of probe **1** under miscellaneous conditions. The addition of **1** to a mixture of four proteins different from hCAI effectively (haemoglobin, bovine serum albumin, concanavaline A and chymotrypsin) did not give a sharp signal. However, the ^{19}F signal was observed clearly in a mixture that contained the four proteins and hCAI (Supplementary Fig. 1b). We also found that the hCAI-induced appearance of the ^{19}F signal occurred with a 70% fetal bovine serum solution, which contains many biological substances, including proteins, lipids and small molecules (Supplementary Fig. 1c). Overall, these results clearly demonstrate that probe **1** can detect hCAI selectively by a turn-on ^{19}F signal, even in crude samples.

The self-assembly/disassembly properties of probe **1** were investigated with various techniques. Atomic force microscopy (AFM) was used to observe spherical or oval aggregates of **1** with a size that ranged from 200 to 500 nm in diameter (Fig. 2a). Transmission electron microscopy (TEM) and scanning electron microscopy (SEM) data showed the formation of aggregates of approximately 200 nm in size (Fig. 2b and Supplementary Fig. 2a). The ultraviolet–visible absorption spectrum of **1** in a buffer solution showed a broad visible-light scattering around 500–700 nm because

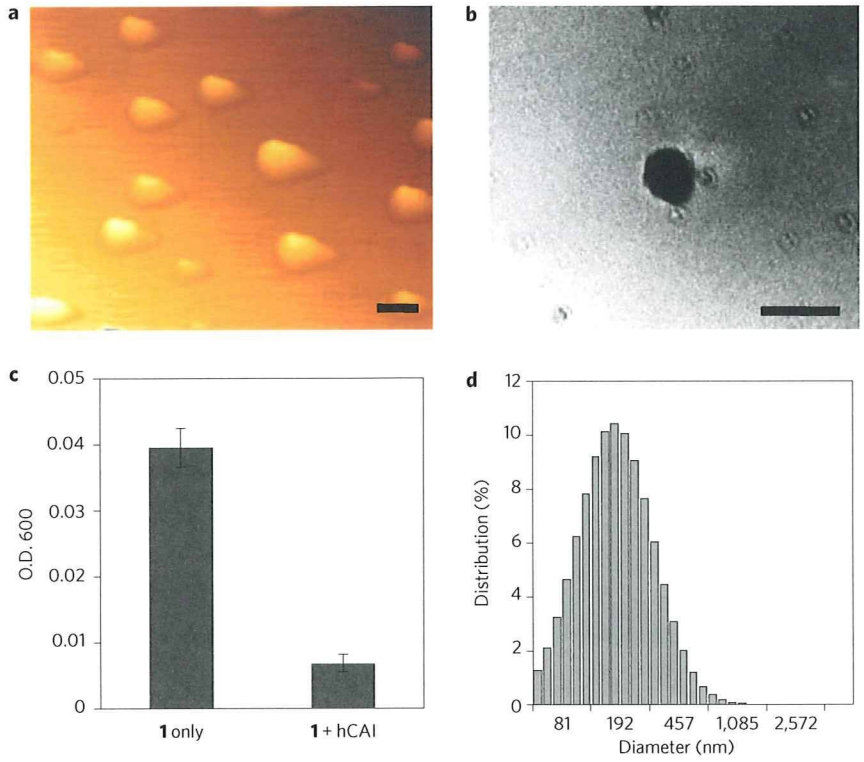

Figure 2 | Microscopic and spectroscopic characterization of the self-assembled nanoparticles of probe 1. a, AFM image of the self-assembled probe **1** (25 μM) (scale bar 500 nm). **b**, TEM image of the self-assembled probe **1** (25 μM) (scale bar 500 nm). **c**, Optical density (O.D.) at 600 nm of an aqueous solution that contained probe **1** (25 μM) in the absence or presence of hCAI (25 μM). Experiments were performed in triplicate to obtain mean and standard deviation values (shown as error bars). **d**, DLS analysis of particle-size distribution of the self-assembled probe **1** (25 μM). All experiments were performed in 50 mM HEPES buffer (pH 7.2, 0.2 mM TFA).

of the aggregates of **1** (Fig. 2c and Supplementary Fig. 2b). The scattering decreased tenfold with the addition of hCAI, which indicates that hCAI collapsed the aggregates. Dynamic light scattering (DLS) measurements in buffer solution that contained **1** alone consistently showed aggregates with a diameter of mean size 250 nm (Fig. 2d), whereas negligible DLS intensity was obtained after adding hCAI to the solution. The M_r of the nanoaggregate of **1** was estimated from the observed diameter to be roughly 10^7 Da, and that of the complex between hCAI and probe **1** to be 3×10^4 Da. We thus conclude that the binding of probe **1** to hCAI induces the disassembly of the nanoaggregates, which dramatically decreases the apparent M_r. This decrease effectively reduces the ^{19}F relaxation rate, so that a sharp ^{19}F signal is observed. From the concentration dependency of DLS measurements, the critical aggregation concentration of the self-assembly of **1** was found to be <5 μM (Supplementary Fig. 2c).

On the basis of this, we next produced a turn-on ^{19}F probe, **3**, for trypsin (TPS). Instead of benzenesulfonamide, benzamidine (**4**), a typical inhibitor for TPS (K_d = ca. 20 μM (ref. 15)), was linked to the 3,5-bis(trifluoromethyl)benzene moiety as a suitable ligand. In NMR spectroscopy, almost no signal was detected in the buffer solution that contained probe **3** alone, whereas a new signal was intensified on the addition of TPS (Fig. 3a). In the presence of **4** (Fig. 1c), such signal intensification did not occur. Similarly, with ^{19}F NMR spectroscopy the biotin-tethered probe **5** showed a clear off/on response to a non-enzymatic protein, avidin (Fig. 3b) (K_d of (+)-biotin (**6**), ca. 10^{-15} M (ref. 16)). Furthermore, the orthogonality of probes **1** and **5** was investigated. It was shown that **1** responded to hCAI, but not to avidin, and vice versa for **5** (Supplementary Fig. 3). These data demonstrate the general applicability of this strategy to the design of turn-on supramolecular nanoprobes to detect target proteins by ^{19}F NMR spectroscopy.

Notably, probe **1** was also capable of detecting hCA within live cells. hCA is a cytosolic protein and naturally expressed within human red blood cells (RBCs) at a concentration of approximately 170 μM (ref. 17). A suspension of RBCs was incubated with **1** for a few minutes and, after collecting cells, in-cell ^{19}F NMR spectroscopy was conducted. Note that no haemolysis occurred during the experiments. A signal was clearly observed at −62.6 ppm (Fig. 4a, spectrum **i**), a chemical shift identical to that obtained using purified hCAI and **1** (Fig. 1d), although there was a slight peak broadening. In contrast, no signal appeared when **1** was incubated with RBCs in

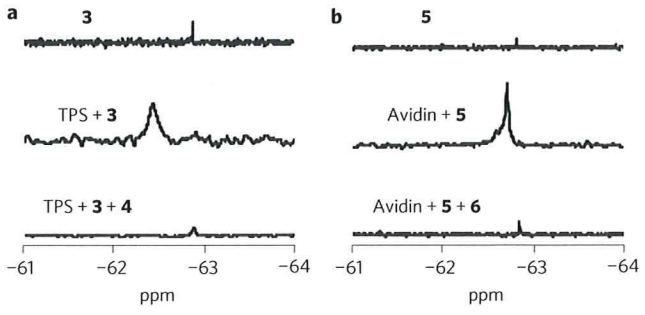

Figure 3 | Turn-on ^{19}F NMR detection of TPS and avidin by probes 3 and 5, respectively. a, ^{19}F NMR spectra of **3** (100 μM) alone, in the presence of TPS (50 μM) and in the presence of both TPS and **4** (500 μM) in 50 mM tris-HCl buffer (pH 8.5, 0.2 mM TFA, 300 mM NaCl, 10% D_2O (v/v)). The SNR was 12.2. **b**, ^{19}F NMR spectra of **5** (100 μM) alone, in the presence of avidin (50 μM) and in the presence of both avidin and **6** (500 μM) in 50 mM HEPES buffer (pH 7.2, 0.2 mM TFA, 500 mM NaCl, 10% D_2O (v/v)). The SNR was 57.3.

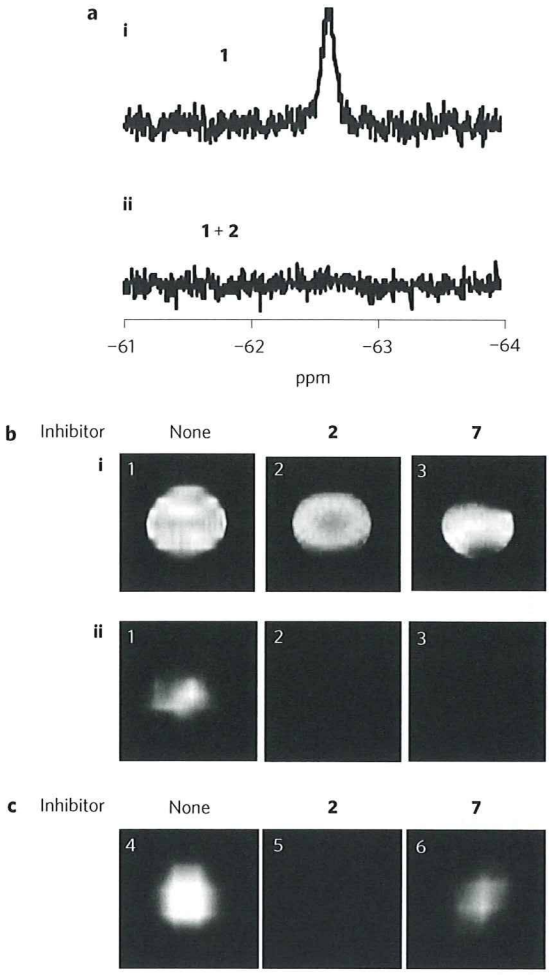

Figure 4 | ^{19}F NMR spectra and magnetic resonance images in RBCs. **a**, ^{19}F NMR spectra of probe **1** in the absence (**i**) or presence (**ii**) of **2** in RBCs. The SNR was 14.2. **b**, Magnetic resonance images (**i**, ^{1}H; **ii**, ^{19}F) of probe **1** in a test tube. **c**, Magnetic resonance images of probe **1** in RBCs. Conditions for samples 1-3: **1** (100 μM), hCAI (50 μM), inhibitors (**2** or **7**) (0 or 500 μM) in 50 mM HEPES buffer (pH 7.2, 0.2 mM TFA). Conditions for samples 4-6: a solution of probe **1** (200 μM) and inhibitors (0 or 1 mM) in 2 ml HEPES buffer saline (20 mM HEPES, 107 mM NaCl, 6 mM KCl, 1.2 mM $MgSO_4$, 2 mM $CaCl_2$, 11.5 mM glucose, pH 7.4) was added to a 2.5 ml RBC suspension. For all samples, after centrifugation the supernatant was removed and the sedimented RBCs were resuspended in 50 mM HEPES buffer (pH 7.2, 100 mM NaCl, 0.17 mM TFA, 20% D_2O (v/v)) and subjected to NMR or MRI measurements at 25 °C.

the presence of **2** (Fig. 4a, spectrum **ii**). Clearly, probe **1** is cell-permeable and can detect endogenous hCA specifically with the turn-on signal response, even within cells.

Turn-on probe **1** allowed us to visualize the target protein using a ^{19}F MRI phantom. At first, ^{1}H and ^{19}F magnetic resonance images were acquired after mixing hCAI with probe **1** under test-tube conditions in the absence (sample 1) and presence (sample 2) of inhibitor **2** or 4-sulfamoylbenzoic acid[13] (**7**, Fig. 1c) (sample 3). In ^{1}H MRI, all three samples gave indistinguishable images (Fig. 4b, image **i**). However, a distinct ^{19}F magnetic resonance image was obtained from sample 1, whereas no signal was detected in samples 2 and 3 (Fig. 4b, image **ii**). These results are consistent with the ^{19}F NMR spectroscopic data described above (Fig. 1d and Supplementary Fig. 1a). More significantly, a clear ^{19}F magnetic resonance image was observed with sample 4, which contained RBCs and probe **1** (Fig. 4c). The magnetic resonance image was diminished totally by co-incubation of **2** (sample 5), which confirms that the positive magnetic resonance image obtained is, indeed, because probe **1** was bound to hCAI within the cells. Interestingly, sample 6, which contained RBCs, probe **1** and **7**, still gave a magnetic resonance image similar to that of sample 4, despite the presence of the inhibitor. Given that **7** efficiently blocks the binding of probe **1** to hCAI under test-tube conditions (Fig. 4b, image **ii**), this result is reasonably ascribed to the lower cell-membrane permeability of anionic **7** compared with that of neutral **2**. Therefore, this system serves as a cell-based inhibitor-screening platform that can visualize the potency of inhibitors in cellular contexts.

Conclusions

In conclusion, we have developed supramolecular ^{19}F-containing nanoprobes that can detect specific proteins spatially by a ^{19}F MRI technique with a sharp turn-on/off switching. The simple principle for the off/on response (that is, self-assembly and recognition-driven disassembly of the nanoprobe[18]) should be applicable to the design of other turn-on probes for various target proteins by appropriately replacing the ligand module, as shown for TPS probe **3** and avidin probe **5**. Unlike other MRI contrast techniques[1–6,11], this method does not require any metals that have potential toxicity. From a practical viewpoint, the sensitivity of ^{19}F MRI is considerably lower than that of ^{1}H MRI and thus this system is not yet sufficient for *in vivo* or clinical application using conventional bench-top spectrometers (which, generally, have strengths of ~1 tesla). Functional ^{19}F probes are also very limited in number. However, we believe that, with further advances in both instrumentation and chemistry, a ^{19}F-based NMR–MRI technique may become a more powerful modality, both in practical diagnosis and in basic research. It is essential for chemists to establish general and useful design concepts for new ^{19}F probes that facilitate functional and molecular MRI.

Methods

^{19}F NMR spectroscopy of probe 1 with various concentrations of hCAI. hCAI (5.0 mg) was dissolved in 50 mM HEPES buffer (1.0 ml, pH 7.2, 10% D_2O (v/v), 0.2 mM TFA). The concentration of hCAI was determined by absorbance at 280 nm using the molar extinction coefficient (49,000 M^{-1} cm^{-1}) (ref. 19) and a 100 μM stock solution was prepared. Probe **1** (3.0 mg, 3.8 μmol) was dissolved in 75 μl of dimethylsulfoxide (DMSO) as the stock solution, and slowly added to the hCAI solution (0.6% DMSO (v/v)). These samples were analysed by ^{19}F NMR spectroscopy with TFA as an internal standard (−75.6 ppm) (Supplementary Methods).

Atomic force microscopy, transmission electron microscopy and scanning electron microscopy observations. In AFM imaging, a solution of probe **1** was spin-coated onto a freshly cleaved mica surface and dried *in vacuo*. Images of the sample were obtained with a tapping-mode AFM on a SEIKO SPA-400 microscope. In TEM imaging, a solution of probe **1** was deposited on a thin carbon-support film and dried *in vacuo*. Images of the sample were obtained with a JEOL JEM-1025 microscope, operating at 100 kV, without any contrast agent. In SEM imaging, a solution of probe **1** was deposited on a silicon wafer and dried *in vacuo*. Images of the sample were obtained with a JEOL JFC-1600 microscope, operating at 15 kV, with the addition of platinum spray as a conductive material.

Measurements of optical density and dynamic light scattering. The optical density was measured at 25 °C in 50 mM HEPES buffer (pH 7.2, 0.2 mM TFA) using a quartz cell (1 cm). The DMSO stock solution of probe **1** was slowly added to the buffer solution (0.6% DMSO (v/v)) to give 25 μM. The measurements of DLS were performed under the same conditions with a tubular-type cell. All measurements were performed in triplicate.

^{19}F NMR spectroscopy of probe 3 and probe 5. TPS (5.0 mg) was dissolved in 50 mM tris-HCl buffer (1.0 ml, pH 8.5, 300 mM NaCl, 0.2 mM TFA, 10% D_2O (v/v)). The concentration of TPS was determined by the absorbance at 280 nm using the molar extinction coefficient (36,700 M^{-1} cm^{-1}) (ref. 20) and a 100 μM stock solution was prepared. Probe **3** (1.0 mg, 1.3 μmol) was dissolved in 26 μl of DMSO and 26 μl of 50 mM tris-HCl buffer (pH 8.5) as the stock solution (25 mM), and slowly added to the TPS solution (0.2% DMSO (v/v)). Avidin (5.0 mg) was dissolved in 50 mM HEPES buffer (1.0 ml, pH 7.2, 500 mM NaCl, 0.2 mM TFA, 10% D_2O (v/v)). The concentration of avidin was determined by the absorbance at 280 nm using the molar extinction coefficient (35,700 M^{-1} cm^{-1}) (ref. 21) and 100 μM stock solution was prepared. Probe **5** (3.0 mg, 3.8 μmol) was dissolved in 72 μl of DMSO as the stock solution, and slowly added to the avidin solution

(0.6% DMSO (v/v)). Conditions used for ^{19}F NMR spectroscopy were the same as those used for probe **1**.

Assays of hCA inhibitor in red blood cells. A 2 ml solution of probe **1** (200 μM) and inhibitor (**2**, 0 or 1 mM, or **7**, 0 or 1 mM) in HEPES buffer saline (20 mM HEPES, 107 mM NaCl, 6 mM KCl, 1.2 mM $MgSO_4$, 2 mM $CaCl_2$, 11.5 mM glucose, pH 7.4) was added to 2 ml of sedimented RBCs, and the suspension was incubated at room temperature for a few minutes. After centrifugation (1,500 revolutions per minute for five minutes), the supernatant was removed and re-suspended in buffer (50 mM HEPES buffer (pH 7.2), 100 mM NaCl, 0.17 mM TFA, 20% D_2O (v/v)) for ^{19}F NMR spectroscopy. 0.7 ml and 2.5 ml of the suspension were used for ^{19}F NMR spectroscopy and MRI, respectively, at 25 °C.

^{1}H and ^{19}F MRI in test tubes or in RBCs. ^{1}H magnetic resonance images of samples 1–3 (in test tubes) were obtained by gradient-spin echo with repetition time (TR)/echo time (TE) = 100/6 ms, flip angle = 30°, field of view (FOV) = 16 × 4 cm, slice thickness = 5 mm, matrix size = 256 × 256 and the number of accumulation (NA) = 1. ^{19}F magnetic resonance images of sample 1–3 (in test tubes) were obtained by fast-spin echo with TR/TE = 1,500/5.5 ms, echo train length = 32, FOV = 16 × 4 cm without slice selection, matrix size = 128 × 32, depth of sample tube = 20 mm, voxel size ~31 mm^3 and NA = 1,200. ^{19}F magnetic resonance images of samples 4–6 (in RBCs) were obtained by gradient-spin echo with TR/TE = 1,000/2.4 ms, flip angle = 90°, FOV = 32 × 8 cm without slice selection, matrix size = 128 × 32, depth of sample tube = 30 mm, voxel size ~188 mm^3 and NA = 400. The sine window function was applied to the ^{19}F magnetic resonance images. All the images were acquired at 25 °C.

Received 14 April 2009; accepted 6 August 2009; published online 23 September 2009

References

1. Kiessling, F., Morgenstern, B. & Zhang, C. Contrast agents and applications to assess tumor angiogenesis *in vivo* by magnetic resonance imaging. *Curr. Med. Chem.* **14,** 77–91 (2007).
2. Perez, J. M., Josephson, L., O'Loughlin, T., Högemann, D. & Weissleder, R. Magnetic relaxation switches capable of sensing molecular interactions. *Nature Biotechnol.* **20,** 816–820 (2002).
3. Louie, A. Y. *et al. In vivo* visualization of gene expression using magnetic resonance imaging. *Nature Biotechnol.* **18,** 321–325 (2000).
4. Sosnovik, D. E. & Weissleder, R. Emerging concepts in molecular MRI. *Curr. Opin. Biotech.* **18,** 4–10 (2007).
5. Woods, M., Woessner, D. E. & Sherry A. D. Paramagnetic lanthanide complexes as PARACEST agents for medical imaging. *Chem. Soc. Rev.* **35,** 500–511 (2006).
6. Jun, Y., Lee, J-H. & Cheon, J. Chemical design of nanoparticle probes for high-performance magnetic resonance imaging. *Angew. Chem. Int. Ed.* **47,** 5122–5135 (2008).
7. Danielson, M. A. & Falke, J. J. Use of ^{19}F NMR to probe protein structure and conformational changes. *Annu. Rev. Biophys. Biomol. Struct.* **25,** 163–195 (1996).
8. Yu, J., Kodibagkar, V. D., Cui, W. & Mason, R. P. ^{19}F: a versatile reporter for non-invasive physiology and pharmacology using magnetic resonance. *Curr. Med. Chem.* **12,** 819–848 (2005).
9. Higuchi, M. *et al.* ^{19}F and ^{1}H MRI detection of amyloid β plaques *in vivo*. *Nature Neurosci.* **8,** 527–533 (2005).
10. Yu, J., Liu, L., Kodibagkar, V. D., Cui, W. & Mason, R. P. Synthesis and evaluation of novel enhanced gene reporter molecules: detection of β-galactosidase activity using ^{19}F NMR of trifluoromethylated aryl β-D-garactopyranosides. *Bioorg. Med. Chem.* **14,** 326–333 (2006).
11. Mizukami, S. *et al.* Paramagnetic relaxation-based ^{19}F MRI probe to detect protease activity. *J. Am. Chem. Soc.* **130,** 794–795 (2008).
12. Grage, S. L. *et al.* Solid state ^{19}F NMR parameters of fluorine-labeled amino acids. Part II: Aliphatic substituents. *J. Magn. Reson.* **191,** 16–23 (2008).
13. Taylor, P. W., King, R. W. & Burgen, A. S. V. Kinetics of complex formation between human carbonic anhydrases and aromatic sulfonamides. *Biochemistry* **9,** 2638–2645 (1970).
14. Casini, A. *et al.* Carbonic anhydrase inhibitors: SAR and X-ray crystallographic study for the interaction of sugar sulfamates/sulfamides with isozymes I, II and IV. *Bioorg. Med. Chem. Lett.* **13,** 841–845 (2003).
15. Talhout, R., Villa, A., Mark, A. E. & Engberts, J. B. F. N. Understanding binding affinity: a combined isothermal titration calorimetry/molecular dynamics study of the binding of a series of hydrophobically modified benzamidinium chloride inhibitors to trypsin. *J. Am. Chem. Soc.* **125,** 10570–10579 (2003).
16. Green, N. M. The use of [^{14}C]biotin for kinetic studies and for assay. *Biochem. J.* **89,** 585–591 (1963).
17. Casey, J. R. *et al.* Carbonic anhydrase inhibitors. Design of selective, membrane-impermeant inhibitors targeting the human tumor-associated isozyme IX. *J. Med. Chem.* **47,** 2337–2347 (2004).
18. Savariar, E. N., Ghosh, S. González, D. C. & Thayumanavan, S. Disassembly of noncovalent amphiphilic polymers with proteins and utility in pattern sensing. *J. Am. Chem. Soc.* **130,** 5416–5417 (2008).
19. Chazalette, C. *et al.* Carbonic anhydrase inhibitors. Design of anticonvulsant sulfonamides incorporating indane moieties. *Bioorg. Med. Chem. Lett.* **14,** 5781–5786 (2004).
20. Talhout, R. & Engberts, J. B. F. N. Thermodynamic analysis of binding of *p*-substituted benzamidines to trypsin. *Eur. J. Biochem.* **268,** 1554–1560 (2001).
21. Finn, F. M., Titus, G., Montibeller, J. A. & Hofmann, K. Hormone-receptor studies with avidin and biotinylinsulin–avidin complexes. *J. Biol. Chem.* **255,** 5742–5746 (1980).

Acknowledgements

We thank E. Ashihara (Kyoto University Hospital) for the blood samples, J. Miyake and T. Kunita (Kyoto University) for help with AFM and SEM measurements. Y.T. acknowledges the JSPS Research Fellowships for Young Scientists. This work was partly supported by CK integrated Medical Bio-imaging Project (MEXT) and by CREST (Japan Science and Technology Agency).

Author contributions

I.H. conceived the project. Y.T., T.S., S.T. and I.H. designed the experiments. Y.T. performed all the experiments, with help from H.T. and M.S. on ^{19}F NMR measurements. M.N. and T.M. performed the MRI experiments. The manuscript was written by Y.T., S.T. and I.H., and edited by all the co-authors.

Additional information

Supplementary information and chemical compound information accompany this paper at www.nature.com/naturechemistry. Reprints and permission information is available online at http://npg.nature.com/reprintsandpermissions/. Correspondence and requests for materials should be addressed to I.H.

J|A|C|S COMMUNICATIONS

Published on Web 10/20/2009

Monitoring of Biological One-Electron Reduction by ^{19}F NMR Using Hypoxia Selective Activation of an ^{19}F-Labeled Indolequinone Derivative

Kazuhito Tanabe,*,† Hiroshi Harada,‡,§ Michiko Narazaki,|| Kazuo Tanaka,⊥ Kenichi Inafuku,⊥ Hirokazu Komatsu,† Takeo Ito,† Hisatsugu Yamada,†,§ Yoshiki Chujo,⊥ Tetsuya Matsuda,|| Masahiro Hiraoka,‡,§ and Sei-ichi Nishimoto*,†

Department of Energy and Hydrocarbon Chemistry, Graduate School of Engineering, Kyoto University, Katsura Campus, Nishikyo-ku, Kyoto 615-8510, Japan, Department of Radiation Oncology and Image-applied Therapy, Graduate School of Medicine, Kyoto University, Shogoin, Sakyo-ku, Kyoto 606-8507, Japan, Nano-Medicine Merger Education Unit, Kyoto University, Shogoin, Sakyo-ku, Kyoto 606-8507, Japan, Department of Systems Science, Graduate School of Informatics, Kyoto University, Yoshida-Honmachi, Sakyo-ku, Kyoto 606-8501, Japan, and Department of Polymer Chemistry, Graduate School of Engineering, Kyoto University, Katsura Campus, Nishikyo-ku, Kyoto 615-8510, Japan

Received June 18, 2009; E-mail: tanabeka@scl.kyoto-u.ac.jp; nishimot@scl.kyoto-u.ac.jp

Intracellular reductases have been closely linked with activation of certain drugs and probes in the tumor-specific microenvironments.[1] Among various enzymes, reductases that catalyze one-electron reduction are involved in the selective activation of functional compounds or materials under hypoxia,[2] a well-known pathophysiological characteristic of solid tumors.[3] Such an enzymatic one-electron reduction has been recognized to be a useful reaction applicable to the design of a tumor hypoxia targeting and imaging strategy. Thus, further quantitative insights into the features of this reaction are important.

Here we demonstrate probing of the biological one-electron reduction of a fluorine (F)-labeled indolequinone (IQ) derivative by ^{19}F NMR that gave us straightforward molecular information even under complicated biological reduction conditions due to low concentrations of endogenous F atoms and the absence of interference with proton signals.[4−6] The family of IQ compounds is well characterized to be superior substrates for several reductases expressed in tumor cells and readily undergoes enzymatic one-electron reduction under hypoxic conditions. Consequently, IQ derivatives have been employed to develop bioreductive prodrugs and imaging probes targeting tumor hypoxia[7,8] that are efficiently activated by endogenous reductase to release a given functional component selectively under hypoxic conditions. We prepared an ^{19}F NMR signal supplier (IQ-F) consisting of a hypoxia-sensitive IQ parent unit and a nonafluoro-*tert*-butyl group and monitored the change in ^{19}F chemical shift during the bioreduction. One-electron reduction of IQ-F by isolated or intracellular reductase under hypoxic conditions released the nonafluoro-*tert*-butyl alcohol (F-OH) constituent. We observed a new ^{19}F signal due to the resultant F-OH at a characteristic chemical shift, which differed from that of IQ-F. In contrast, the release of F-OH was efficiently suppressed upon addition of O_2 and thereby the corresponding signal failed to appear. Kinetic studies indicated that O_2 prevented to a lesser extent the binding of IQ-F to reductase but decreased the rate of the net reaction due to oxidation of a semiquinone anion radical intermediate generated during the course of the one-electron reduction into the parent IQ-F. In addition, the present reaction could be monitored by chemical shift selective fast spin echo (FSE),[9] leading to visualization of the hypoxia-selective reduction by signal intensity using MR imaging.

† Department of Energy and Hydrocarbon Chemistry.
‡ Department of Radiation Oncology and Image-applied Therapy.
§ Nano-Medicine Merger Education Unit.
|| Department of Systems Science.
⊥ Department of Polymer Chemistry.

IQ-F was synthesized by coupling 3-hydroxymethyl-5-methoxy-1,2-dimethylindole-4,7-dione with F-OH (Scheme S1). We conducted the enzymatic reduction of IQ-F in an Ar-purged aqueous acetonitrile solution by means of NADPH:cytochrome P450 reductase, which catalyzes the one-electron reduction of quinone derivatives to semiquinone anion radicals.[7a] We incubated IQ-F with NADPH:cytochrome P450 reductase and its cofactor β-NADPH under hypoxic conditions. Figure 1 shows the reaction of IQ-F monitored by ^{19}F NMR. The appearance of a single new signal at −73.6 ppm during hypoxic treatment is attributable to the formation of F-OH, as confirmed by reference to authentic sample, while the IQ-F starting compound almost completely disappeared (Figure 1B). These results clearly indicate that IQ-F is activated to release the corresponding alcohol F-OH by enzymatic reduction, thereby causing a change in the ^{19}F NMR spectra. In contrast, upon enzymatic treatment under aerobic conditions, a substantial amount of IQ-F remained to produce a negligible signal attributable to F-OH (Figure 1C). Thus, enzymatic reduction of IQ-F occurred in a hypoxia-selective manner, as can be monitored by ^{19}F NMR.[10]

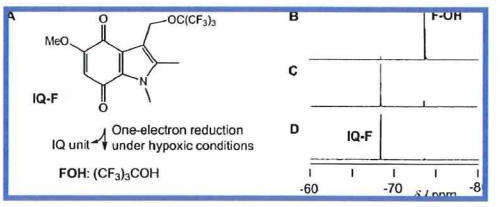

Figure 1. (A) Bioreduction of IQ-F under hypoxic conditions to release F-OH. (B, C, D) One-electron reduction of IQ-F monitored by ^{19}F NMR. IQ-F (0.93 mM) was incubated with NADPH:cytochrome P450 reductase (11.4 μg) and β-NADPH (2 mM) at 37 °C in phosphate buffer; (B) incubated for 15 min under hypoxic conditions; (C) incubated for 15 min under aerobic conditions; and (D) before incubation.

The steady-state kinetic parameters, V_{max} and K_m, for the release of F-OH were derived from a Lineweaver−Burk plot[11] of the integration values evaluated in the ^{19}F NMR spectra (Figure S1). The V_{max} value for F-OH formation under aerobic conditions (0.20 ± 0.04 pmol min^{-1}) was considerably lower than that under hypoxic conditions (3.1 ± 0.2 pmol min^{-1}), while the K_m value obtained from hypoxic treatment (0.41 ± 0.04 mM) was similar to that from aerobic treatment (0.59 ± 0.16 mM). Thus, binding of IQ-F to reductase was slightly affected by the oxygen concentration, while the net reaction rate was dramatically reduced in the presence of O_2. These characteristics are consistent with the conventional mechanism hitherto proposed for IQ

10.1021/ja904953b CCC: $40.75

derivatives. A semiquinone anion radical intermediate is generated under both hypoxic and aerobic conditions by enzymatic one-electron reduction of IQ. The resulting intermediate is subject to oxidization by O_2 to regenerate the original IQ along with the formation of $O_2^{-\bullet}$ under aerobic conditions, leading to significant suppression of the net reaction. The enzymatic activation of IQ-F, which leads to an NMR signal change, is likely to occur substantially under hypoxic conditions.

To better understand the function of IQ-F in living cells, we also assessed the one-electron reduction of IQ-F in a human cell line of lung carcinoma A549 cells that express NADPH:cytochrome P450 reductase in high amounts.[12,13] A549 cells were cultured in the presence of IQ-F for 12 h under hypoxic or aerobic conditions. The culture medium and the cell lysate were individually harvested and subjected to an NMR study. In a similar manner to the treatment of IQ-F with isolated reductase, a signal originating form the formation of F-OH was observed in the medium obtained upon incubation under hypoxic conditions, as shown in Figure 2A. We also confirmed that a weak F-OH signal was produced upon aerobic treatment. In a control experiment, no signal was observed in the corresponding cell lysates independent of oxygen concentrations (Figure S2). Therefore IQ-F most likely penetrates into living cells where it is activated to release F-OH by intracellular reductases in a hypoxic environment, while it is promptly eliminated from cells due to the small size of the molecule, resulting in the low concentration of the intracellular F-signal supplier, which was below the detection limit.

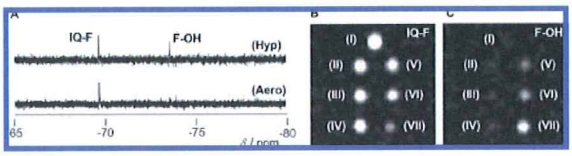

Figure 2. (A) One-electron reduction of IQ-F in A549 cells. A549 cells were incubated with IQ-F (355 μM) for 12 h under hypoxic (Hyp) or aerobic (Aero) conditions. The medium obtained from the reaction sample was subjected to an ^{19}F NMR study. (B,C) ^{19}F MR images of IQ-F incubated with cell lysate of A549 for 0 (I), 6 (II and V), 12 (III and VI), and 24 h (IV and VII) under aerobic (II, III, and IV) or hypoxic (V, VI, and VII) conditions: (B) IQ-F signal selected image; (C) F-OH signal selected image.

To confirm whether the reduction can occur within cells, we further studied the reaction of IQ-F upon treatment with cell lysate. An aqueous solution of IQ-F containing 6% CD_3CN was incubated at 37 °C under hypoxic or aerobic conditions with the lysate of A549 cells. We observed that the ^{19}F NMR signal of F-OH increased in a time-dependent manner only during treatment under hypoxic conditions (Figure S3), indicating that hypoxia-selective one-electron reduction of IQ-F by intracellular reductase is responsible for an exclusive NMR signal change.

In light of the above reaction characteristics of IQ-F, attempts were also made to monitor the reaction of IQ-F by means of MR imaging, a technique widely employed in medical diagnosis.[14] We employed ^{19}F chemical shift selected imaging[9] for probing of the one-electron reduction of IQ-F. IQ-F was incubated under hypoxic and aerobic conditions with the lysate of A549 cells. As shown in Figure 2B and 2C, ^{19}F images of IQ-F and F-OH were obtained individually and simultaneously by FSE with a chemical shift selective pulse.[15] Upon aerobic treatment, an intense IQ-F signal remained, while no F-OH signal was detected even after prolonged incubation. It is striking that the F-OH signal increased with increasing time upon hypoxic treatment, along with a concomitant decrease in IQ-F signals. In accord with the evidence that incubation of IQ-F in a buffer resulted in a similar ^{19}F image as in the sample incubated under aerobic conditions (Figure S5), the hypoxia-selective one-electron reduction of IQ-F could be clearly monitored by ^{19}F MR imaging.

In conclusion, the hypoxia-selective one-electron reduction of IQ-F, which consists of a hypoxia-sensitive IQ parent unit and an ^{19}F signal-transmitting molecular unit of nonafluoro-*tert*-butyl group, was characterized by ^{19}F NMR. During monitoring of the biological reduction of IQ-F, hypoxia-selective activation occurred to induce a chemical shift change of ^{19}F signals attributable to the reductive formation of F-OH. The disappearance of IQ-F to form F-OH could be imaged simultaneously by ^{19}F FSE, thus visualizing the occurrence of the enzymatic one-electron reduction in a hypoxia-selective manner by means of MR imaging.

The one-electron reduction of IQ derivatives has been widely used for hypoxia targeting and imaging. The IQ-F activation system could be applicable to MR imaging of tumor hypoxia. Optimization of the chemical structure of IQ-F derivatives to increase water solubility and intracellular retention and characterization of their pharmacokinetic profiles are now in progress.

Acknowledgment. This work is partly supported by the Innovative Techno-Hub for Integrated Medical Bioimaging Project of the Special Coordination Funds for Promoting Science and Technology, from the Ministry of Education, Culture, Sports, Science and Technology (MEXT), Japan and by the Program for Promotion of Fundamental Studies in Health Sciences of the National Institute of Biomedical Innovation (NIBIO), Japan.

Supporting Information Available: Detail of synthetic protocol and enzymatic reduction of IQ-F. This material is available free of charge via the Internet at http://pubs.acs.org.

References

(1) (a) Chen, Y.; Hu, L. *Med. Res. Rev.* **2009**, *29*, 29. (b) Colucci, M. A.; Moody, C. J.; Couch, G. D. *Org. Biomol. Chem.* **2008**, *6*, 637.
(2) Tanabe, K.; Zhang, Z.; Ito, T.; Hatta, H.; Nishimoto, S. *Org. Biomol. Chem.* **2007**, *5*, 3745.
(3) (a) Kizaka-Kondoh, S.; Inoue, M.; Harada, H.; Hiraoka, M. *Cancer Sci.* **2003**, *94*, 1021. (b) Harris, A. L. *Nat. Rev. Cancer* **2002**, *2*, 38.
(4) (a) Zimmermann, U.; Nöth, U.; Gröhn, P.; Jork, A.; Ulrichs, K.; Lutz, J.; Haase, A. *Artif. Cells, Blood Substitutes, Immobilization Biotechnol.* **2000**, *28*, 129. (b) Yu, J.; Kodibagkar, V. D.; Cui, W.; Mason, R. P. *Curr. Med. Chem.* **2005**, *12*, 819. (c) Higuchi, M.; Iwata, N.; Matsuba, Y.; Sato, K.; Sasamoto, K.; Saido, T. C. *Nat. Neurosci.* **2005**, *8*, 527. (d) Ahrens, E. T.; Flores, R.; Xu, H. Y.; Morel, P. A. *Nat. Biotechnol.* **2005**, *23*, 983.
(5) (a) Tanaka, K.; Kitamura, N.; Naka, K.; Chujo, Y. *Chem. Commun.* **2008**, 6176. (b) Mizukami, S.; Takikawa, R.; Sugihara, F.; Hori, Y.; Tochio, H.; Waelchli, M.; Shirakawa, M.; Kikuchi, K. *J. Am. Chem. Soc.* **2008**, *130*, 794. (c) Cui, W.; Otten, P.; Li, Y.; Koeneman, K. S.; Yu, J.; Mason, R. P. *Magn. Reson. Med.* **2004**, *51*, 616. (d) Oishi, M.; Sumitani, S.; Nagasaki, Y. *Bioconjugate Chem.* **2007**, *18*, 1379.
(6) For recent reports on detecting the effects of reductases, see: (a) Robinson, S. P.; Griffiths, J. R. *Philos. Trans. R. Soc. London, Ser. B* **2004**, *359*, 987. (b) Krohn, K. A.; Link, J. M.; Mason, R. P. *Int. J. Nucl. Med.* **2008**, *49*, 129S. (c) Salmon, H. W.; Siemann, D. W. *Radiother. Oncol.* **2004**, *73*, 359.
(7) (a) Tanabe, K.; Hirata, N.; Harada, H.; Hiraoka, M.; Nishimoto, S. *ChemBioChem* **2008**, *9*, 426. (b) Zhang, Z.; Tanabe, K.; Hatta, H.; Nishimoto, S. *Org. Biomol. Chem.* **2005**, *3*, 1905.
(8) (a) Hernick, M.; Flader, C.; Borch, R. F. *J. Med. Chem.* **2002**, *45*, 3540. (b) Everett, S. A.; Swann, E.; Naylor, M. A.; Stratford, M. R. L.; Patel, K. B.; Tian, A.; Newman, R. G.; Vojnovic, B.; Moody, C. J.; Wardman, P. *Biochem. Pharmacol.* **2002**, *63*, 1629. (c) Swann, E.; Barraja, P.; Oberlander, A. M.; Gardipee, W. T.; Hundnott, A. R.; Beall, H. D.; Moody, C. J. *J. Med. Chem.* **2001**, *44*, 3311.
(9) (a) Kimura, A.; Narazaki, M.; Kanazawa, Y.; Fujiwara, H. *Magn. Reson. Imag.* **2004**, *22*, 855. (b) Kuribayashi, H.; Doi, Y.; Kanazawa, Y. *Magn. Reson. Med.* **2001**, *46*, 864.
(10) We observed slow reduction of IQ-F during the treatment with NQO1 that catalyzes two-electron reduction independent of the presence of oxygen. Therefore, IQ-F may not be an ideal substrate for NQO1. See Figure S6.
(11) Moore, W. J. *Physical Chemistry*; Prentice-Hall, Inc.: NJ, 1972.
(12) Yu, L. J.; Matis, J.; Scudiero, D. A.; Hite, K. M.; Monk, A.; Sausville, E. A.; Waxman, D. J. *Drug Metab. Dispos.* **2001**, *29*, 304.
(13) To prepare an aqueous solution of IQ-F, we employed a solubilization kit for hydrophobic drugs (PUREBRIGHT).
(14) McRobbie, D. W.; Moore, E. A.; Graves, M. J.; Prince, M. R. *MRI From Picture to Proton*; Cambridge University Press: Cambridge, 2003.
(15) An experimental detail was illustrated in Figure S4. See also Experimental Section described in the Supporting Information.

JA904953B

Journal of Applied Microbiology ISSN 1364-5072

ORIGINAL ARTICLE

Evaluation of a new medium for the enumeration of total coliforms and *Escherichia coli* in Japanese surface waters

H. Kodaka[1,2], S. Mizuochi[1], M. Saito[2] and H. Matsuoka[2]

1 Research Institute of Advanced Technology, Nissui Pharmaceutical Co. Ltd, Hokunanmoro, Yuki, Ibaraki, Japan
2 Department of Biotechnology and Life Science, Tokyo University of Agriculture and Technology, Nakamachi, Koganei, Tokyo, Japan

Keywords
coliforms, EC-Blue-10, *E. coli*, enumeration, MPN, water.

Correspondence
Hidemasa Kodaka, Research Institute of Advanced Technology, Nissui Pharmaceutical Co. Ltd, 1075-2, Hokunanmoro, Yuki, Ibaraki 307-0036, Japan.
E-mail: h-kodaka@yki.nissui-pharm.jp

2007/0564: received 10 April 2007, revised and accepted 20 September 2007

doi:10.1111/j.1365-2672.2007.03627.x

Abstract

Aim: A new medium, EC-Blue-10, containing chromogenic and fluorogenic substrates, KNO_3 and sodium pyruvate has been developed for the rapid simultaneous detection and enumeration of total coliforms and *Escherichia coli* in water.

Methods and Results: Two evaluations of EC-Blue-10 were carried out. Firstly, EC-Blue-10 was compared with Colilert-MPN for 96 water samples using MPN for total coliforms and *E. coli*. Secondly, the detection of coliforms and *E. coli* were compared using 2400 tubes of EC-Blue-10 and Colilert-MPN. The regression coefficients between EC-Blue-10 and Colilert-MPN for total coliforms and *E. coli* were 0·91 and 0·89, respectively. For the detection results, the Cohen's kappa values between the two media were 0·79 for coliforms and 0·72 for *E. coli*.

Conclusions: EC-Blue-10 is almost same as Colilert-MPN for the detection of coliforms and *E. coli* in surface waters. Further evaluation for EC-Blue-10 is needed to verify in different geographical areas.

Significance and Impact of the Study: EC-Blue-10 is useful method for the rapid and simultaneous detection of total coliforms and *E. coli* in water sample.

Introduction

Total coliforms and *Escherichia coli* are important indicators of the sanitary quality of drinking water. The standard test for the coliform group is either the multiple-tube fermentation technique (Grasso *et al.* 2000) or the membrane-filter technique (Bernasconi *et al.* 2006). Since traditional multiple-tube fermentation and membrane-filter methods require a minimum of 24 h incubation followed by a confirmation procedure lasting 24–48 h, there is a requirement for rapid test methods for the emergency testing of drinking water supplies. During recent decades new chromogenic or fluorogenic, defined substrate methods based on β-galactosidase for total coliforms or β-glucuronidase for *E. coli* and ready-made culture media have been introduced (Edberg and Edberg 1988). Many chromogenic media based on β-galactosidase for total coliforms use *o*-nitrophenol-β-D-galactopyranoside (ONPG) or chlorophenol red-β-D-galactopyranoside (CPRG) as a substrate. The results of studies comparing media containing ONPG or CPRG and 4-methylumbelliferyl-β-D-glucuronide (MUG) with standard methods (Edberg *et al.* 1988; Buckalew *et al.* 2006) provide critical information confirming the accuracy of the defined substrate technology (DST) method, its comparability to a standard method, and its applicability for use. ONPG could be replaced successfully by 5-bromo-4-chloro-3-indoxyl-β-D-galactopyranoside (X-Gal) (Manafi and Kneifel 1989). However, there are few studies testing commercially available liquid media that use X-Gal and MUG for the simultaneous determination of total coliforms and *E. coli* in water (Manafi and Kneifel 1989; Geissler *et al.* 2000; Hörman and Hänninen 2006). We have developed a new medium using X-Gal and MUG for rapidly and simultaneously detecting total coliforms and *E. coli* in water. EC-Blue-10 is a new medium in a special

plastic disposable tube sterilized by electron beam. After incubation at 35°C for 24 h, the development of a blue-green colour in an initially light yellow-coloured solution demonstrates the presence of coliforms and fluorescence at 366 nm in the same tube demonstrates the presence of *E. coli*. Since a DST method has been used as a Japanese standard method since 1992 (Japan Water Works Association [JWWA] 2001), it was decided to use this DST method to confirm the validity of EC-Blue-10 for rapidly and simultaneously detecting coliforms and *E. coli* in temperate humid climate zone waters sampled in Japan.

Materials and methods

EC-Blue-10

EC-Blue-10 consists of a granulated medium in a special plastic bottle sterilized by electron beam. The medium was developed primarily for the rapid growth of *Enterobacteriaceae* (Kodaka *et al.* 1995) and contains the following ingredients g l^{-1}: Trypticase peptone (Becton, Dickinson and Company, Sparks, MD, USA) 5·0, NaCl 5·0, K_2HPO_4 4·0, KH_2PO_4 1·0, KNO_3 1·0, sodium pyruvate 1·0, sodium dodecyl sulphate (SDS) 0·1, MUG 0·1, X-Gal 0·1, isopropyl-β-D-thiogalactopyranoside 0·1 and pH 7·1 ± 0·2.

Effect of media for the detection of coliform bacteria from chlorinated water sample

Escherichia coli American Type Culture Collection (ATCC, VA, USA) 11775, *Citrobacter freundii* ATCC 8090, *Enterobacter cloacae* ATCC 13047 and *Klebsiella pneumoniae* ATCC 13883 were used in this study. Each coliform bacterium was suspended in sterilized phosphate buffer saline (PBS) solution prepared to make 20 000 CFU 400 ml^{-1} in 500 ml Erlenmeyer flask. The bacteria suspension was kept in the water bath at 20°C until mixing with chlorine solution. The chlorine solution was prepared to a target concentration of 0·3 mg l^{-1} (0·3 ppm) in 400 ml sterilized PBS solution in 500 ml Erlenmeyer flask. The chlorine solution was kept in the water bath at 20°C until mixing with the bacterial suspension. The 400 ml bacterial suspension and 400 ml chlorine solution were mixed promptly in 1000 ml sterilized brown Erlenmeyer flask with stopper. This mixed solution was stirred by stirring bar and 100 ml mixed solution was taken at 15, 30, 60, 120 and 300 s after adding sodium hypochlorite (NaOCl) into 300 ml sterilized Erlenmeyer flask containing 0·5 ml of 1 mol l^{-1} of sodium thiosulfate. Each 50 ml sample was diluted with 450 ml sterilized PBS solution. About 10 ml of diluted sample was inoculated into 10 tubes of EC-Blue-10, Colilert-MPN, Lactose Broth with bromothymol blue (LB: Nissui Pharmaceutical Co. Ltd, Tokyo, Japan) and Brilliant Green Lactose Bile broth (BGLB: Nissui Pharma.). These cultures were incubated at 36 ± 1°C for 48 h. During the 48-h incubation, the positive reaction was observed at 20, 24, 28 and 48 h. This experiment was done three times for each strain. The comparison for detection of each coliform from chlorinated water samples was carried out to sum up the positive results from the data of three experiments.

Influence of heterotrophic bacteria for coliforms and *E. coli* detection

Each coliform bacterium (*E. coli* ATCC 11775, *Cit. freundii* ATCC 8090, *Ent. cloacae* ATCC 13047 and *Kl. pneumoniae* ATCC 13883) was suspended in 250 ml sterilized PBS solution to make 20 CFU ml^{-1}. Three heterotrophic bacteria [*Flavobacterium odoratum* Japan Collection of Micro-organisms (JCM, Saitama, Japan) 7458, *Acinetobacter calcoaceticus* JCM 6842 and *Pseudomonas aeruginosa* from JWWA] were mixed and suspended in 250 ml PBS solution to make 60 000 CFU ml^{-1}. Each coliform bacterium and the heterotrophic suspension were mixed in equal volumes. The mixed bacterial suspension was inoculated into 10 tubes of two media and incubated at 35°C. The positive reaction was observed at 20, 24, 28 and 48 h. The experiments were done in duplicate for each coliform bacterium.

Evaluation procedure for untreated and chlorinated natural water

The natural water samples were collected by eight water-work stations following the instructions issued by JWWA between September (average temperature: 24·4°C at Tokyo) and October (average temperature: 20·1°C at Tokyo) 1998. Ten-litre water samples were collected in sterilized bottles and were kept in the dark and at a cool temperature (5°C) until examination. The examinations were carried out within 48 h of collection. Each water sample was tested in duplicate on the same day. The water samples were put into sterilized 3000 ml Erlenmeyer flasks and stirred with a magnetic stirrer at 20 ± 1°C. The following procedure was carried out in accordance with the instructions of JWWA. NaOCl solution was added to give a concentration of 0·2 mg l^{-1} for lake-waters and 0·5 mg l^{-1} for river-waters. The sampling time after the addition of NaOCl was 20, 60, 180, 300 and 1800 s. Each water sample was then put into sterilized 300 ml Erlenmeyer flasks containing 1 mol l^{-1} of sodium thiosulfate. Total coliforms and *E. coli* in each of the 16 untreated and 80 chlorinated natural water samples (total 96 water samples) were then estimated using EC-Blue-10 and Colilert-MPN (Colilert, IDEXX Laboratories, KK, Tokyo,

Japan) by the five-tube, five-dilution MPN method. Each medium was incubated at 36 ± 1°C. The results were read at 24 h for total coliforms and *E. coli*. The presence of coliforms using EC-Blue-10 was identified by the development of a blue-green colour in an initially light yellow coloured solution and the presence for *E. coli* was identified by the development of fluorescence at 366 nm in the same vessel. For Colilert-MPN, the development of a yellow colour indicated the presence of coliforms and fluorescence on exposure to long-wavelength UV light denoted the presence of *E. coli*.

Isolation and identification

The presence of total coliforms was confirmed by identifying the bacterial isolate(s) to species level from at least one positive EC-Blue-10 and Colilert-MPN tube per row according to the method of Edberg *et al.* (1988). The isolation of bacteria was carried out by streaking onto Levine–Eosin Methylene Blue agar (L-EMB, Becton, Dickinson and Company). Colonies with a typical green metallic sheen, representative of each morphology present, were picked and re-streaked on XM-G agar (the agar medium containing 5-bromo-6-chloro-3-indoxyl-β-D-galactopyranoside (Magenta-Gal) and 5-bromo-4-chloro-3-indoxyl-β-D-glucuronic acid, cyclohexylammonium salt (X-Gluc), Nissui Pharma.) and incubated for 24 h at 35°C. Presumptive identification for coliforms and *E. coli* was confirmed by Magenta-Gal and X-Gluc reactions on XM-G agar, respectively. Bacterial isolates were inoculated onto plate count agar to confirm the purity of cultures. The isolates for identification were selected after due consideration of geographical differentiation, sampling time and colony morphology on L-EMB and XM-G agar. Gram-negative rods were identified by API 20E system (bioMerieux Japan Ltd, Tokyo, Japan) and ID TEST EB-20 (Nissui Pharma.) (Kodaka *et al.* 2004). The identification of all isolates was also confirmed by standard methods.

Tests for microbial and physical properties

The tests were done according to the Japanese Standard Methods for Examination of Water (JWWA 1993). The standard plate count (SPC) using plate count agar incubated at 36 ± 1°C for 24 ± 2 h and the heterotrophic plate count (HPC) using PYG agar (g l^{-1}: peptone 2·0, glucose 0·5, yeast extract 1·0, agar 15, pH 7·0 ± 0·1) incubated at 20 ± 1°C for 7 days were carried out before adding NaOCl. The residual chlorine was measured using the *N,N*-diethyl-*p*-phenylenediamine method. The turbidity was measured with a turbidimeter (ANA-7S Tokyo, Koden, Tokyo, Japan) comparing the sample with a kaolin turbidity standard solution [1 mg of kaolin in 1000 ml of distilled water has a turbidity of approx. one nephelometric turbidity units (NTU)]. The water temperature was measured with Celsius liquid-in-glass thermometer. The pH was measured with a pH meter (HM-60V, TOA Electronics, Tokyo, Japan) with a glass electrode.

Statistical analysis

Total results for the 96 sets of MPN data were calculated as $\log_{10}$ MPN of total coliforms and *E. coli* 100 ml^{-1} of water samples. Statistical calculations were carried out with the MICROSOFT EXCEL 2000 statistics package. The statistical analysis consisted of regression analysis and paired *t*-test for the MPN data. The chi-square test and Cohen's kappa for homogeneity of presence/absence results were compared using 2400 tubes of EC-Blue-10 and Colilert-MPN, respectively. All statistical analyses were performed with a level of significance of 0·05. The data were also analysed according to the ISO 17994 (2004) for the establishment of equivalence between EC-Blue-10 and Colilert-MPN methods, prescribes calculation of 100-times the logarithmic (ln) difference. The evaluation of equivalence is based on the mean and the expanded uncertainty derived from the standard uncertainty of the mean.

Results

Effect of media for coliform bacteria from chlorinated water sample

No difference between 24 and 48 h for positive reactions were observed among four media. Therefore, we have compared the cultures for positive reaction at 24 h incubation. A total of 30 tubes were examined at each chlorine treatment time. For the detection of *E. coli* ATCC 11775 after chlorine treatment for 15, 30, 60, 120 and 300 s, positive X-Gal tubes of EC-Blue-10 were 6, 4, 9, 3 and 0, respectively, and positive ONPG tubes of Colilert-MPN were 11, 4, 11, 1 and 1, respectively. Positive MUG tubes of EC-Blue-10 were 6, 4, 9, 3 and 0, respectively, and positive MUG tubes of Colilert-MPN were 10, 2, 11, 1 and 1, respectively. The positive gas production tubes of LB were 19, 15, 18, 4 and 3, respectively. The positive gas production tubes of BGLB were 16, 10, 16, 3 and 0, respectively. For the detection *Cit. freundii* ATCC 8090, positive X-Gal tubes of EC-Blue-10 were 29, 29, 21, 7 and 1, respectively, and positive ONPG tubes of Colilert-MPN were 30, 30, 25, 7 and 5, respectively. The positive gas production tubes of LB were 30, 30, 13, 12 and 4, respectively. The positive gas production tubes of BGLB were 27, 12, 3, 3 and 0, respectively. For the detection of *Ent. cloacae* ATCC 13047, positive X-Gal tubes of EC-Blue-10 were 15, 7, 4, 2 and 0, respectively, and positive ONPG

tubes of Colilert-MPN were 6, 3, 4, 1 and 0, respectively. No positive tubes for gas production in LB and BGLB were observed. For the detection of *Kl. pneumoniae* ATCC 13883, positive X-Gal tubes of EC-Blue-10 were 27, 27, 26, 9 and 12, respectively, and positive ONPG tubes of Colilert-MPN were 3, 5, 3, 1 and 1, respectively. The positive gas production tubes of LB were 25, 29, 28, 20 and 23, respectively. The positive gas production tubes of BGLB were 19, 21, 23, 14 and 12, respectively. MUG reaction in each medium was not observed with *Cit. freundii* ATCC 8090, *Ent. cloacae* ATCC 13047 and *Kl. pneumoniae* ATCC 13883.

Heterotrophic bacterial influence to detect coliforms and *E. coli*

The heterotrophic bacteria at 10^4 CFU level found in these samples appeared neither to interfere with coliforms and *E. coli* detection nor to account for the differences between EC-Blue-10 and Colilert-MPN in coliforms and *E. coli* detection. Mixtures of the heterotrophic bacteria did not result in false-negative analyses.

Untreated and chlorinated natural water samples

A total of 96 MPN tests for each water sample and each NaOCl exposure time were carried out using EC-Blue-10 and Colilert-MPN. The results of the regression analyses for total coliforms are shown in Table 1. Median $\log_{10}$ MPN 100 ml^{-1} ± standard deviation (SD) for total coliforms with EC-Blue-10 and Colilert-MPN were 2·11 ± 1·32 and 2·23 ± 1·38, respectively. The regression coefficient, slope and intercept between EC-Blue-10 and Colilert-MPN were 0·91, 0·96 and −0·0012, respectively (Table 1). The results of the regression analyses for *E. coli* are shown in Table 1. Median $\log_{10}$ MPN 100 ml^{-1} ± SD for *E. coli* with EC-Blue-10 and Colilert-MPN were 0 ± 0·91 and 0 ± 0·89, respectively. The regression coefficient, slope and intercept between EC-Blue-10 and Colilert-MPN were 0·89, 0·85 and 0·084, respectively. The means of MPN results for total coliforms and *E. coli* with EC-Blue-10 and Colilert-MPN were not statistically significantly different ($P > 0·05$) by paired *t*-test. For all comparisons, the slope and intercept values, as determined by linear regression analysis, were close to 1·00 and 0·00, respectively. The presence/absence results using 2400 tubes of EC-Blue-10 and Colilert-MPN were compared. For the coliform test, the results were 959 positive tubes of EC-Blue-10 and 925 positive tubes of Colilert-MPN (Table 2). For the *E. coli* test 208 tubes were positive using EC-Blue-10 and 217 tubes were positive using Colilert-MPN (Table 2). These results indicated no significant difference between the two media using the chi-square test ($P > 0·05$). The substantial agreements between the two kits obtained using Cohen's kappa were 0·79 for total coliforms and 0·72 for *E. coli*. Table 3 shows statistical evaluations of the equivalence of the two methods for total coliforms and *E. coli* according to ISO 17994 (2004). Samples were excluded from calculations when both methods gave zero (0, 0). The expanded uncertainty was derived from the standard uncertainty of the mean by using the coverage factor $k = 2$. The evaluation for results of the comparison and the confidence interval of the expanded uncertainty around the mean was calculated by computing the lower limit (x_L) and upper limit (x_H). The x_L and x_H for total coliforms and *E. coli* were −3·0 and 51·6 and −44·9 and 44·3, respectively. Assuming that the maximum acceptable deviation (D) has been chosen as D = 10%. The means of relative difference for total

Table 1 Parameters of each test for total coliforms and *Escherichia coli* from water samples*

	Total coliforms		*E. coli*	
Parameters	EC-Blue-10	Colilert-MPN	EC-Blue-10	Colilert-MPN
No. of tested samples	96	96	96	96
No. of positive samples	93	87	37	41
Median ($\log_{10}$ MPN/100 ml)	2·11	2·23	0	0
SD ($\log_{10}$ MPN/100 ml)	1·32	1·38	0·91	0·89
95% Confidence limit	0·26	0·28	0·18	0·18
Regression coefficient	0·91		0·89	
Slope	0·96		0·85	
Intercept	−0·0012		0·084	
t†	1·75		−0·17	
df	95		95	

*Include 16 untreated and 80 chlorinated water samples.
†Paired *t*-test at the significance level ($P = 0·05$).

Table 2 Comparison of presence/absence results from 2400 tubes for coliforms and *Echerichia coli*

	Coliforms				*E. coli*			
Test kit	Pr*	Ab†	*k*‡	*P*§	Pr*	Ab†	*k*‡	*P*§
EC-Blue-10	959	1441	0·79	0·62	208	2192	0·72	0·10
Colilert-MPN	925	1475			217	2183		

*Pr, presence.
†Ab, absence.
‡*k*, Cohen's kappa value.
§*P*, *P* value by chi-square.

Table 3 Statistical evaluation of the equivalence of the two MPN methods for total coliforms and *Escherichia coli* according to ISO 17994 (2004)

	No. of Samples	n_0*	n†	Mean relative difference	SD	Expanded uncertainty range x_L	Expanded uncertainty range x_H	One-sided evaluation
Total coliforms	96	1	95	24·3	133·0	−3·0	51·6	Inconclusive
E. coli	96	47	49	−0·3	156·0	−44·9	44·3	Inconclusive

*n_0, number of samples excluded because of zero.
†n, number of samples retained for analysis.

Table 4 Statistical evaluation of P/A results according to ISO 17994 (2004)

	*n*A*	*n*B†	x^2‡
Coliform	147	101	8·53
E.coli	49	63	1·75

**n*A, the number of samples where EC-Blue-10 was positive and Colilert-MPN negative.
†*n*B, the number of samples where EC-Blue-10 was negative and Colilert-MPN positive.
‡x^2, Poisson index of dispersion.

coliforms and *E. coli* were 24·3 and −0·3, respectively. The evaluations for total coliforms and *E. coli* in accordance with one-sided evaluation of ISO 17994 (2004) were both 'inconclusive' because the data were insufficient for decisions. Table 4 shows statistical evaluation of P/A results for coliform and *E. coli* according to ISO 17994 (2004). The values of the Poisson-index of dispersion (x^2) for coliform and *E. coli* were 8·53 and 1·75, respectively. EC-Blue-10 and Colilert-MPN methods were considered to be 'different' for coliform, however both methods were considered to be 'not different' in accordance with evaluation for two P/A methods of ISO 17994 (2004).

Bacterial isolates

Table 5 shows species of Gram-negative isolated from untreated and chlorinated water samples. The total number of isolates for identification from EC-Blue-10 and Colilert-MPN were 41 and 46, respectively. The coliforms (excluding *E. coli*) that were isolated from water samples were *Cit. amalonaticus*, *Ent. agglomerans*, *Ent. cloacae*, *Ent. intermedium*, *Kl. Pneumoniae* and *Serratia marcescens*. There were mixed cultures of total coliforms present in both EC-Blue-10 and Colilert-MPN tubes.

Relation between coliforms and bacterial counts

Table 6 shows the microbiological and physical properties of each sample during the experiments. The HPC ranged from 3550 to 140 500 CFU ml^{-1} with PYG agar and the SPC ranged from 1305 to 141 000 CFU ml^{-1} with plate count agar. No relationship was noticed between SPC, HPC and coliforms.

Table 5 Species of Gram-negative identified

Species	% of all isolates identified by EC-Blue-10	% of all isolates identified by Colilert-MPN
Coliforms		
Citrobacter amalonaticus	5	2
Enterobacter agglomerans	13	1
Ent. cloacae	1	9
Ent. intermedium	3	1
Escherichia coli	40	42
Klebsiella pneumoniae	3	9
Serratia liquefaciens	1	2
Ser. marcescens	10	1
Noncoliforms		
Aeromonas caviae	1	2
Morganella morganii	5	2
Providencia alcalifaciens	1	2
Pseudomonas aeruginosa	8	1
Ps. fluorescens	3	4
Ps. putida	5	15
Proteus vulgaris	1	7

Total isolates for identification from EC-Blue-10 and Colilert-MPN were 41 and 46, respectively.

Discussion

Statistical evaluations of the equivalence of the EC-Blue-10 and Colilert-MPN methods for total coliforms and *E. coli* according to one-sided evaluation of ISO 17994 (2004) were 'inconclusive' for total coliforms and *E. coli*. About 25 additional samples for total coliforms and about 1000 additional samples for *E. coli* would have been sufficient numbers to reach firm decisions. The ONPG test with the ONPG peptone-water medium is preferable for growth of the organisms (Lowe 1962). EC-Blue-10 contains biological material such as peptone for the enhanced growth for bacteria, whereas Colilert-MPN is minimal medium for bacteria. Two ingredients of

Table 6 Microbial and physical properties of each water sample during the experiments

Sampling areas	No. of coliforms isolated		No. of *E.coli* isolated		SPC* (CFU ml^{-1})	HPC† (CFU ml^{-1})	Free Cl^-(mg l^{-1})	Total Cl^-(mg l^{-1})	Temp. (°C)	NTU‡	pH
	EC- Blue-10	Colilert- MPN	EC-Blue-10	Colilert-MPN							
A-lake	25	17	4	4	1305	2563	0·1	0·2	21·1	0·6	7·3
B-river	31	38	12	16	21700	120500	0·2	0·4	20·5	2·9	7·4
C-river	26	20	6	6	141000	140500	0·3	0·5	20·1	0·5	7·4
D-lake	46	35	14	5	1118	3550	0·1	0·2	20·8	2·0	8·6
E-river	32	34	8	11	2503	26575	0·2	0·5	20·0	0·8	7·3
F-river	30	26	11	10	16275	71000	0·4	0·5	19·6	2·6	7·3
G-river	33	34	4	7	1973	6700	0·1	0·3	20·1	1·5	7·6
H-river	43	47	13	25	19950	71000	0·1	0·5	20·3	1·1	7·5
Mean	33	31	9	11	25728	55299	0·2	0·4	20·5	1·5	7·6
SD	8	10	4	7	47408	54313	0·1	0·1	0·5	0·9	0·4

Sixteen untreated and 80 chlorinated water samples were tested.
*SPC, Standard plate count.
†HPC, Heterotrophic plate count.
‡NTU: Nephelometric turbidity units.

EC-Blue-10 are also different from Colilert-MPN. Firstly, EC-Blue-10 contains sodium pyruvate as nonenzyme peroxide-degrading compound to increase the detection of chlorine-stressed coliform bacteria (Sartory 1995). Secondly, the KNO_3 in EC-Blue-10 is important for bacteria, as it allows energy production during nitrate respiration (Hadjipetrou and Stouthamer 1965). Bacteria, commonly considered part of the total coliform group were isolated from both EC-Blue-10 and Colilert-MPN tubes. *E. coli* was isolated from tubes with both positive-colour and -fluorescence. *E. coli* was primarily isolated from water samples, followed by *Ent. agglomerans*, *Kl. pneumoniae* and *Serratia marcescens*. Every isolate was inoculated into both media to confirm the reactions. No different reactions were observed between EC-Blue-10 and Colilert-MPN. There did not appear to be a significant difference in the distribution of bacterial species in either medium. The HPC on most samples were higher than the SPC. Only one sample, C-river, had almost the same microbiological count (Table 6). The results of heterotroph interference study and the results in Table 6 support the notion that heterotrophic bacteria do not interfere with the detection or enumeration of total coliforms and *E. coli* by the EC-Blue-10. After the addition of NaOCl, total coliforms were detected from the H-river water sample using both methods. The microbial and physical properties of this water sample were not significantly different from the other water samples (Table 6). We have not investigated why total coliforms were detected after the addition of NaOCl. There was a concern that bacteria other than *E. coli* might exhibit fluorescence. No false-negative results were observed in this study. However, we did find false-positive results, with β-glucuronidase positive *Staph. warneri* being isolated from EC-Blue-10 and pyoverdin positive *Ps. putida* being isolated from Colilert-MPN. *Staph. warneri* could be resistant to 0·1 g SDS l^{-1} in EC-Blue-10 (Kodaka *et al.* 1995). We agree with Edberg *et al.* (1988) that each test was limited by design to drinking water distribution samples and the user should first establish the efficacy of the test in each water sample. A weak fluorescent reaction for MUG test can be read in the aqueous phase of the medium. A disadvantage of EC-Blue-10 was that it was difficult to read a weak-positive blue colour, because the base colour of EC-Blue-10 is light yellow. However, the medium in EC-Blue-10 was developed primarily for the rapid growth of *Enterobacteriaceae* (Kodaka *et al.* 1995). If coliforms were present in the water sample, they could grow sufficiently. Therefore, it would be very rare to observe a weak reaction and if a weak reaction was observed, it could be confirmed by comparison to the EC-Blue-10 comparator.

In conclusion, EC-Blue-10 gave results that were almost statistically equivalent to the DST method currently accepted by the Ministry of Health, Labour and Welfare of Japan. Therefore, the EC-Blue-10 is as useful as the DST method for the detection of coliforms and *E. coli* in temperate humid climate zone water. However, the water samples tested were very limited in this evaluation of EC-Blue-10 and therefore, it is recommended that a more extensive evaluation of EC-Blue-10 be undertaken.

Acknowledgements

The authors thank JWWA for providing the evaluation protocol and water samples for this study. We also thank Dr Richard Meldrum of Llandough Hospital (Penarth, UK) for critically reading the manuscript.

References

Bernasconi, C., Volponi, G. and Bonadonna, L. (2006) Comparison of three different media for the detection of *E. coli* and coliforms in water. *Water Sci Technol* **54**, 141–145.

Buckalew, D.W., Hartman, L.J., Grimsley, G.A., Martin, A.E. and Register, K.M. (2006) A long-term study comparing membrane filtration with Colilert® defined substrates in detecting fecal coliforms and *Escherichia coli* in natural waters. *J Environ Manage* **80**, 191–197.

Edberg, S.C. and Edberg, M.M. (1988) A defined substrate technology for the enumeration of microbial indicators of environmental pollution. *Yale J Biol Med* **61**, 389–399.

Edberg, S.C., Allen, M.J., Smith, D.B. and the national collaborative study (1988) National field evaluation of a defined substrate method for the simultaneous enumeration of total coliforms and *Escherichia coli* from drinking water: comparison with the standard multiple tube fermentation method. *Appl Environ Microbiol* **54**, 1595–1601.

Geissler, K., Manafi, M., Amorós, I. and Alonso, J.L. (2000) Quantitative determination of total coliforms and *Escherichia coli* in marine waters with chromogenic and fluorogenic media. *J Appl Microbiol* **88**, 280–285.

Grasso, G.M., Sammarco, M.L., Ripabelli, G. and Fanelli, I. (2000) Enumeration of *Escherichia coli* and coliforms in surface water by multiple tube fermentation and membrane filter methods. *Microbiology* **103**, 119–125.

Hadjipetrou, L.P. and Stouthamer, A.H. (1965) Energy production during nitrate respiration by *Aerobacter aerogenes*. *J Gen Microbiol* **38**, 29–34.

Hörman, A. and Hänninen, M.-L. (2006) Evaluation of the lactose Tergitol-7, m-Endo LES, Colilert 18, Readycult Coliforms 100, Water-Check-100, 3M Petrifilm EC and DryCult Coliform test methods for detection of total coliforms and *Escherichia coli* in water samples. *Water Res* **40**, 3249–3256.

ISO 17994 (2004) *Water Quality – Criteria for Establishing Equivalence between Microbiological Methods*. Geneva: International Organization for Standardization.

Japan Water Works Association (1993) *Standard Methods for Examination of Water*. Tokyo, Japan: Japan Water Works Association [in Japanese].

Japan Water Works Association (2001) *Standard Methods for Examination of Water*. Tokyo, Japan: Japan Water Works Association [in Japanese].

Kodaka, H., Ishikawa, M., Iwata, M., Kashitani, F., Mizuochi, S. and Yamaguchi, K. (1995) Evaluation of new medium with chromogenic substrates for members of the family *Enterobacteriaceae* in urine samples. *J Clin Microbiol* **33**, 199–201.

Kodaka, H., Uesaka, Y. and Kashitani, F. (2004) Nissui glucose fermentative gram-negative rod identification system EB-20 gives a unique profile for typical non-sorbitol-fermenting *Escherichia coli* O157:H7. *J Clin Microbiol* **42**, 354–358. [Erratum. *J Clin Microbiol* **42**, 1857].

Lowe, G.H. (1962) The rapid detection of lactose fermentation in paracolon organisms by the demonstration of β-D-galactosidase. *J Med Lab Technol* **19**, 21–25.

Manafi, M. and Kneifel, W. (1989) A combined chromogenic-fluorogenic medium for the simultaneous detection of total coliforms and *E. coli* in water. *Zentralbl Hyg Umweltmed* **189**, 225–234 [in German].

Sartory, D.P. (1995) Improved recovery of chlorine-stressed coliforms with pyruvate supplemented media. *Water Sci Technol* **31**, 255–258.

Biocontrol Science, 2007, Vol. 12, No. 1, 31－34

Note

Automatic Mapping of Viable Microbial Cells Distributed in the Surface Layer of Cotton Fabrics

KOHTARO FUJIOKA[1, 2], IKUKO KOZONE[2], MIKAKO SAITO[2], AND HIDEAKI MATSUOKA[2]*

[1]*Kobe Technical Center, Procter & Gamble Far East, Inc., 17, Koyo-cho Naka 1-Chome, Higashinada-ku, Kobe 658-0032, Japan*

[2]*Department of Biotechnology and Life Science, Tokyo University of Agriculture and Technology, Koganei, Tokyo 184-8588, Japan*

Received 17 October 2006/Accepted 18 January 2007

Viable microbial cells distributed in a 130 μm thick surface layer of cotton fabrics were stained with a fluorescent glucose, 2-[*N*-(7-nitrobenz-2-oxa-1,3-diazol-4-yl)amino]-2-deoxy-D-glucose (2-NBDG), and automatically mapped with an ultra-deep focusing range microscope (UDF) system. The software of the UDF system was upgraded and the number of *Candida albicans* cells could be counted at a higher precision than before. Bacterial cells of *Pseudomonas fluorescens*, *Serratia marcescens*, and *Citrobacter freundii*, which were smaller than 1-2 μm, were successfully mapped for the first time. These results indicate the practical importance of the present method in the evaluation of the antibacterial properties of fabrics and the efficacy of washing.

Key words : Ultra-deep focusing range (UDF) fluorescent microscope/A fluorescent glucose/ Viable cell imaging/Cell deposition on fabrics.

Visualization *in situ* of viable microbial cells on the surface of fabrics is of practical importance and has been important for the evaluation of antibaterial properties of fabrics (JIS L1902, 2002; Borkow and Gabbay, 2004; Cen et al., 2004) and the efficacy of washing (Petrocci and Clarke, 1969; JIS L0844, 1997; ASTM E2274-03, 2004). One of the key challenges in conducting such an evaluation is to deal with the topology of fabric surfaces which is not flat at the micrometer scale but composed of many fibers to form a complex structure. Microbial cells are deposited on thin fibers or entrapped deeply between fibers. To detect these cells within a deep focusing range simultaneously, confocal microscopy (Roldán et al., 2004; Staudt et al., 2004), decomvolution microscopy (McNally et al., 1999), and other methods (Burton, 2003; Buda et al., 2005) have been proposed and in fact some models based on these principles are commercially available. However it was difficult to modify available models at a reasonable cost to fit our specific resolutional purpose. Thus we developed a novel microscopic system with an UDF system (Fujioka et al., 2006). In combination with the staining of viable cells with a fluorescent glucose derivative, 2-NBDG (Yoshioka et al., 1996; Matsuoka et al., 2003), the UDF system was found to be useful for the rapid evaluation of the efficacy of microbial cell removal (EMR) from fabrics in the specific case of *Candida albicans* microbes greater than 5 μm.

From a practical viewpoint, however, it is essential to establish a spatial resolution as high as 1-2 μm. In this study, we have critically revised the principal image processing software. As described below, the mapping of *C. albicans* has been successfully performed with much higher resolution. The mappings of bacterial cells smaller than 1-2 μm are also demonstrated.

Seed cultures of *C. albicans* ATCC10231, the environmental isolates of *Pseudomonas fluorescens*,

*Corresponding author. Tel : +81-42-388-7029, Fax : +81-42-387-1503, e-mail: mhide@cc.tuat.ac.jp

Serratia marcescens, and *Citrobacter freundii* were prepared from respective frozen stocks with MICROBANK kit (Pro-lab Diagnostics, Toronto, Canada) and cultured in 1/10 strength Trypticase Soy Broth (1/10 TSB) to approximately 10^5 cfu/ml. Fabric samples used were Kanakin 3 (JIS L0803, 1998), Cotton knit without a brightener, and Cotton 100 denim. These are differently knitted to form unique textures and certified by the Japan Spinners' Association. The fabric swatches were prepared as 1.0 cm × 1.0 cm squares, wrapped with aluminum foil, autoclaved at 121℃ for 15 min, and dried up under sterilized conditions. The synthesis of 2-NBDG was performed following the protocol described elsewhere (Yoshioka et al., 1996).

A 50 μl inoculum of the seed culture containing about 5×10^5 cells of *C. albicans* was inoculated onto each swatch, and the swatch was placed on Trypticase Soy Agar (TSA) plates. After the incubation at 33℃ for 16 h, each swatch was soaked in 9ml saline and vortexed for 5 min to remove most of the microbial cells from the each swatch. Thus we prepared swatch samples on which only small numbers of microbial cells remained. Each swatch was cut into 2 pieces (0.5 cm×1.0 cm each). One piece (I) was used for the visualization experiment after being stained with 2-NBDG. The other piece (II) was used for the colony count assay only in the case of bacterial cells.

The conditions of 2-NBDG staining were as follows. A 400 μl aliquot of 12 μM 2-NBDG was placed on the fabric swatch piece (I). After incubation at 33℃ for 10 min, the remaining aqueous liquid was removed by Ultrafree-MC centrifuging treatment (6000 rpm × 30s). After that, a 100 μl of 30% formaldehyde (HCHO) solution was added with a pipette on the swatch and incubated at 33℃ for 1 min in order to fix the microbial cells. Immediately after that, the swatch was soaked in 9 ml saline for 5 min and centrifuged (6000 rpm × 30 s) to remove extracellular 2-NBDG. This washing with saline was repeated 2 times and microscopic observation with the UDF system was performed.

Previously we often encountered the image of a *C. albicans* cell indicated by an arrow in Fig. 1. In such a case, the single-cell emitted intense fluorescence at both ends and consequently was recognized as 2 cells in the automatic mapping. Such an image was due to a large vacuole that could hardly be stained by 2-NBDG. The increase in the spatial resolution, however, has enabled the recognition of such a case as a single-cell. Typical cases are observed at 4 positions in Fig. 2-Aa. These spots could be successfully registered as single-cells, respectively, as No. 1, 2, 5, and 8 in Fig. 2-Ab. A similar case is also observed in Fig. 2-Ba and registered as No. 5.

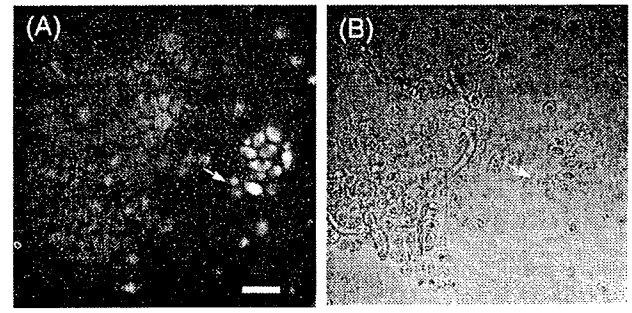

FIG. 1. Typical fluorescent pattern observed in *C. albicans* stained with 2-NBDG. (A) Fluorescent image, (B) Bright field image. Scale bar: 10 μm. The arrow indicates a typical image pattern of both ends emitting intense fluorescence. Observed with VC100×oil objective lens through BV-2A filter.

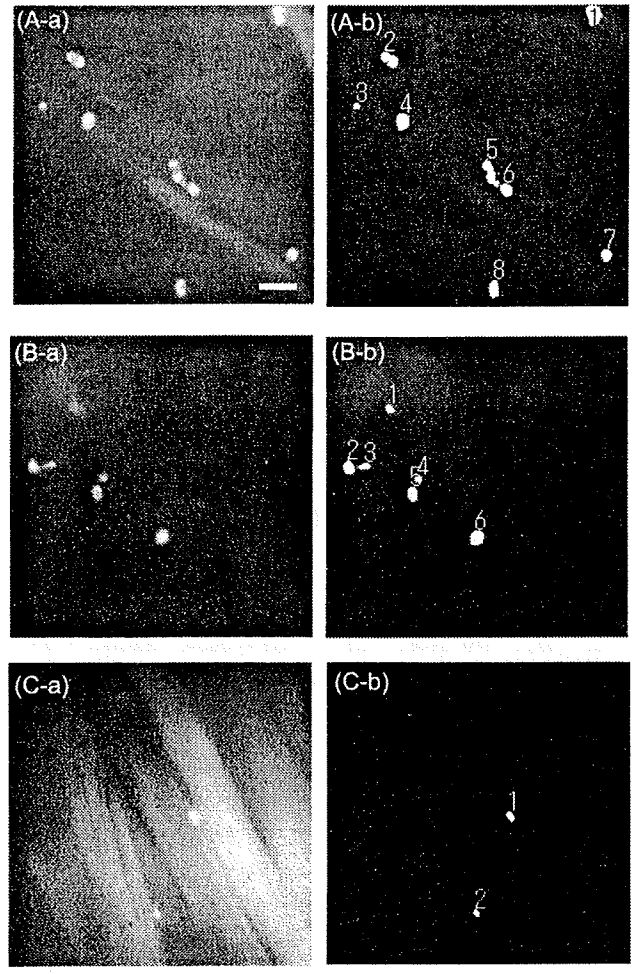

FIG. 2. Mapping of *C. albicans* in the surface layer of different cotton materials. (A) Kanakin3, (B) Cotton Knit without brightener, (C) Cotton 100 Denim. Scale bar: 10 μm.

As may be observed in the Figs. 2-Ab, 2-Bb, and 2-

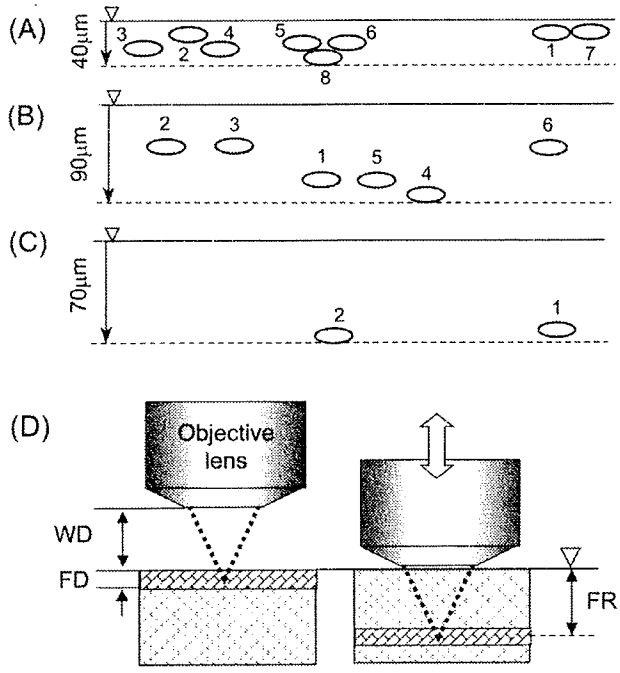

FIG. 3. Estimated depth of each cell from the fabric surface. Numbered cells in (A), (B), and (C) correspond to the numbered cells in (A), (B), and (C) of Fig.2, respectively. (D) Focusing range that can be observed simultaneously by the UDF system. ▽: Fabric surface, - - - in (A)~(C): Deepest cell level observed in respective cases, WD: Working distance (130 μm), FD: In-focus depth (a few μm), FR: Focusing Range (max 130 μm).

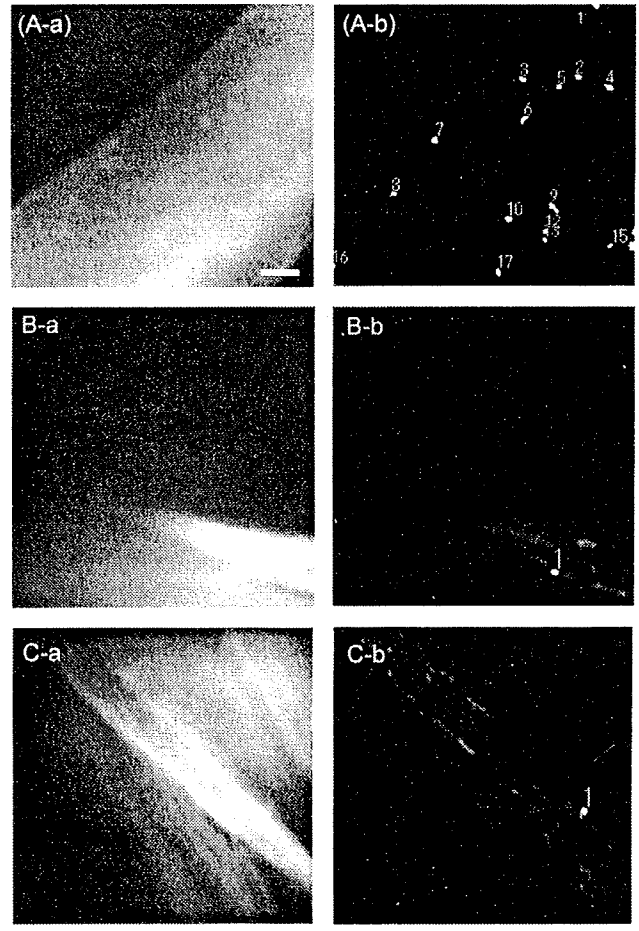

FIG. 4. Mapping of bacterial cells in the surface layer of Kanakin3. (A) *P. fluorescens*, (B) *S. marcescens*, (C) *C. freundii*. Observed with VC100×oil objective lens through BV-2A filter. Scale bar: 10 μm.

Cb, it is noticed that every fluorescent spot looks equally clear in outline and similar in size, though every cell does not necessarily exist in the same depth. The UDF system can integrate microscopic images from the surface to 130 μm depth at maximum (Fig. 3-D). Therefore the mapping data include the information of the depth of each cell. Based on these data, approximate positions of respective cells are shown in Figs. 3-A, 3-B, and 3-C. Such data are useful to estimate the degree of cell invasion into fabric matrices of different physical properties as well as their removal by washing.

Next is the automatic mapping of bacterial cells smaller than 2-3 μm. The objective lens was ×100 APO to zoom into the bacterial cell. In the case of Fig. 4-Aa, many fluorescent spots could be observed with similar fluorescent intensities. Thus every spot could be mapped as a light spot of similar size by adjusting the threshold level for the binarization at an appropriate level (Fig. 4-Ab). In the other two cases, only one cell was recognized as a light spot (Figs. 4-Ba, 4-Ca). According to the properly adjusted threshold level and the criteria for single-cell size, only this spot could be registered as a bacterial cell (Fig. 4-Bb, 4-Cb).

Practically, it is necessary to confirm the quantitative relation between the cell numbers determined by the present method and by the conventional colony count method. However, the challenge of statistics regarding sample size still remained. In fact the area that was analyzed by the present method was too small to be compared to the colony count method. This problem will be resolved by the future development of an automatic scanning system for a fabric swatch of a much larger area.

Since only one cell is detected in Fig.4-B and 4-C respectively, it may be necessary to confirm by the colony count method that bacterial cells were actually remaining on/in the fabric swatch. The other halves (swatch piece (II)) used for Fig. 4 were assayed for viable cells according to the following protocol. The swatch piece (II) was immersed in 9 ml of 1/10 TSB and vortexed for 5 min and then taken out from the 1/10 TSB. A 0.5 ml aliquot of the 1/10 TSB

(suspension A) was mixed with TSA and poured in a dish for culturing at 33℃ for 72 h. Since the cell concentration in the suspension A was thought to be markedly small, suspension A was also incubated at 33℃ for another successive 48 h to increase it. A 100 μl aliquot of the resulting suspension (suspension B) was spread on a TSA plate and incubated at 33 ℃ for 24 h to count the colony number. As a result, after the incubation, no colony growth was observed on the TSA plates of suspension A. On the other hand, some growth was observed on the plates of suspension B (Fig.4-B: 44 cfu/plate, Fig.4-C: 55 cfu/plate). This supports the idea that the amounts of the residual levels of bacteria are very low.

In conslusion, the UDF system has been upgraded so that it may count automatically the cell number of *C. albicans* as well as smaller bacterial cells at a higher precision than before. The present results suggest the importance of the further development of a practical version of the UDF system.

Acknowledgments

This research was supported by the Microbial Visualization Community of Practice of the Procter & Gamble Company. The authors would like to thank Dr. P. Geis and Dr. S. Donaldson of the Procter & Gamble Company for holding constructive discussions with us and for reviewing the manuscript. We also thank Mr. Tottori of Kogaku Inc. for his support for and input into the microscopic system designs. One of the authors, H. Matsuoka, acknowledges support from Grant-in-aid for Scientific Research for the Promotion of Safety and Security of Foods, The Ministry of Health, Labor, and Welfare.

REFERENCES

ASTM E2274-03 (2004) Standard test method for evaluation of laundry sanitizers and disinfectants.

Borkow, G., and Gabbay, J. (2004) Putting copper into action: copper-impregnated products with potent biocidal activities. *FASEB J.*, **18**, 1728-1730.

Buda, A., Sands, C., and Jepson, M.-A. (2005) Use of fluorescence imaging to investigate the structure and function of intestinal M cells. *Adv. Drug Deliv. Rev.*, **57**, 123-134.

Burton, K. (2003) An aperture-shifting light-microscopic method for rapidly quantifying positions of cells in 3D matrices. *Cytometry*, **A54**, 125-131.

Cen, L., Neoh, K.-G., and Kang, E.-T. (2004) Antibacterial activity of cloth functionalized with N-alkylated poly(4-vinylpyridine). *J. Biomed. Mater. Res.*, **A71**, 70-80.

Fujioka, K., Kozone, I., Saito, M., and Matsuoka, H. (2006) Rapid evaluation of the efficacy of microbial cell removal from fabrics. *J. Ind. Microbiol. Biotechnol.*, **33**, 995-1002.

Japan Industrial Standard L0844 (1997) Test methods for colour fastness to washing and laundering.

Japan Industrial Standard L1902 (2002) Testing for antibacterial activity and efficacy on textile products.

Petrocci, A. M., and Clarke, P. (1969) Proposed test method for antimicrobial laundry additives. *J. of AOAC*, **52**, 836-842.

Roldán, M., Thomas, F., Castel, S., Quesada, A., and Hernández-Mariné, M. (2004) Noninvasive pigment identification in single cells from living phototrophic biofilms by confocal imaging spectrofluorometry. *Appl. Environ. Microbiol.*, **70**, 3745-3750.

Staudt, C., Horn, H., Hempel, D.-C., Neu, T.-R. (2004) Volumetric measurements of bacterial cells and extracellular polymeric substance glycoconjugates in biofilms. *Biotechnol. Bioeng.*, **88**, 585-592.

Matsuoka, H., Oishi, K., Watanabe, M., Kozone, I., Saito, M., and Igimi, S. (2003) Viable cell detection by the combined use of fluorescent glucose and fluorescent glycine. *Biosci. Biotechnol. Biochem.*, **67**, 2459-2462.

McNally, J.-G., Karpova, T., Cooper, J., and Conchello, J.-A. (1999) Three-dimensional imaging by deconvolution microscopy. *Methods*, **19**, 373-385.

Yoshioka, K., Takahashi, H., Homma, T., Saito, M., Oh, K.-B., Nemoto, Y., and Matsuoka, H. (1996) A novel fluorescent derivative of glucose applicable to the assessment of glucose uptake activity of *Escherichia coli*. *Biochim. Biophys. Acta*, **1289**, 5-9.

J Ind Microbiol Biotechnol (2007) 34:685–688
DOI 10.1007/s10295-007-0231-7

SHORT COMMUNICATION

Visualization of yeast single-cells on fabric surface with a fluorescent glucose and their isolation for culture

Kohtaro Fujioka · Philip Geis · Mikako Saito · Hideaki Matsuoka

Received: 25 March 2007 / Accepted: 20 May 2007 / Published online: 14 June 2007

Abstract An ultra-deep focusing range (UDF) fluorescent microscope system has been combined with a micromanipulation system to develop a viable cell detection-identfication system applicable to microbes on environmental surfaces and products. *Candida albicans* yeast cells on a fabric sample surface were viably stained with a fluorescent glucose derivative, 2-[*N*-(7-nitrobenz-2-oxa-1,3-diazol-4-yl)amino]-2-deoxy glucose (2-NBDG) and detected with a UDF fluorescent microscope. Visualized single-cells of *C. albicans* were picked in a glass microcapillary and transferred onto an agar medium. After the culture, the colony was assayed for DNA sequence to identify the isolate. This demonstrates a potential application to the study of unknown environmental microorganisms.

Keywords Ultra-deep focusing range (UDF) fluorescent microscope · Single-cell manipulation · Fluorescent glucose derivative · Viable cell imaging

K. Fujioka
Kobe Technical Center, Procter & Gamble Far East, Inc., 17, Koyo-cho Naka 1-Chome, Higashinada-ku, Kobe 658-0032, Japan

K. Fujioka · M. Saito · H. Matsuoka (✉)
Department of Biotechnology and Life Science, Tokyo University of Agriculture and Technology, Koganei, Tokyo 184-8588, Japan
e-mail: bio-func@cc.tuat.ac.jp

P. Geis
Sharon Woods Technical Center, The Procter & Gamble Co., 11530 Reed Hartman Highway, Cincinnati, OH 45242, USA

Introduction

Quantitative and qualitative analyses of environmental microorganisms have been attempted with various methods and approaches [2, 3, 7, 13, 15]. Where effective, these usually require days to obtain the results and fail to connect the visual to microbial species. Currently, urgent needs exist in the detection of food pathogens in cooking environment [11, 17] and microbial growth in damp garments after the laundry washing process [10, 14]. To meet these needs, we have recently developed a ultra-deep focusing range (UDF) fluorescent microscope system and applied it successfully to the evaluation of microbial cell removal from fabrics [4], and to the automatic mapping of viable microbial cells being distributed in the surface layer of cotton fabrics [5]. The next step is to isolate those single-cells for their identification. Once the single-cells have been isolated, they can be cultured on an agar medium. Thus formed colonies may be used for further investigation including DNA analysis and metabolism analysis. This research demonstrates the detection of single-cells of *Candida albicans* on fabrics and their isolation for the culture.

Materials and methods

Microbial strains

Candida albicans, which is one of the key human pathogens [6, 16] and contaminants in cosmetic industry [1] was chosen as a microbial strain for this study. Seed cultures of *C. albicans* ATCC 10231 were prepared from frozen stocks from MICROBANK kit (Pro-lab Diagnostics, Toronto, Canada) and cultured in the 1/10th strength Trypticase Soy Broth (1/10 TSB) to approximately 10^6 cfu/ml. Fabric